Ore Geology Reviews 100 (2018) 334–346

Contents lists available at ScienceDirect

Ore Geology Reviews

journal homepage: www.elsevier.com/locate/oregeorev

Geology, geochemistry and genesis of the Zankan iron deposit in the West Kunlun Orogen, Xinjiang, China

Zhen-Ju Zhou[a,b], Hao-Shu Tang[c,*], Yan-Shuang Wu[d], Qiu-Gen Li[b], Yan-Jing Chen[b,*], Zheng-Le Chen[a]

[a] Institute of Geomechanics, Chinese Academy of Geological Sciences, Beijing 100081, China
[b] Key Laboratory of Orogen and Crustal Evolution, Peking University, Beijing 100871, China
[c] State Key Laboratory of Ore Deposit Geochemistry, Institute of Geochemistry, Chinese Academy of Sciences, 46 Guanshui Road, Guiyang 550002, China
[d] Xinjiang Research Center for Mineral Resources, Xinjiang Institute of Ecology and Geography, Chinese Academy of Sciences, Urumqi 830011, China

ARTICLE INFO

Keywords:
Sulfur isotope
Magnetite-sulfide-sulfate assemblage
Zankan iron deposit
Seafloor hydrothermal system
West Kunlun Orogen

ABSTRACT

The Zankan iron deposit (Taxkorgan County, Xinjiang) is a recently discovered large Fe deposit in western China. The deposit is hosted in the Bulunkuole metamorphic complex in the Taxkorgan terrane of the West Kunlun Orogen. The ores are uniquely composed of magnetite, pyrite and anhydrite with variable contents, and show massive, disseminated and banded styles. The ores contain widely varying (Al_2O_3 + TiO_2) (0.28–5.48 wt%), Zr (3.0–83 ppm) and Hf (< 0.2–2 ppm), indicating a terrigenous clastic material input. Detrital contamination is minor, as demonstrated by poor correlations of Y/Ho ratio vs. Zr, Th, Hf and Al_2O_3 contents, as well as Zr vs. TiO_2. The ores contain seawater-like LREE depletion, positive La and Y anomalies, and occasional Eu enrichment, which suggest hydrothermal contributions. In addition, three samples show relatively high REY (604–1254 ppm), negative Eu anomalies (Eu/Eu^*_{PAAS} = 0.36–0.96) and MREE enrichment (Sm/Yb_{PAAS} = 1.25–2.81), suggesting a probable fluvial input and shallow precipitation. The $\delta^{34}S$ ratios range widely (3.2–32.8‰) and show an alternating and/or mixing source of two end-members. The seawater sulfate may have been an indispensable end-member, and the other end-member may have been the volcanic host rocks in the Bulunkuole Complex, which has likely contributed the ore-forming metals. Integrating evidence from regional geology, ore geology, and geochemistry, we conclude that the Zankan Fe deposit was the result of an Early Cambrian seafloor hydrothermal system.

1. Introduction

Located on the southwestern margin of the Tarim Craton, the recently discovered Taxkorgan iron belt lies between the West Kunlun Orogen and Pamir Plateau, western China (Fig. 1A and B). The belt contains over ten iron deposits, with a total resource of 1.556 Bt Fe (Fig. 1C) (Dong et al., 2011, 2012). Hosted in the metamorphosed volcanic and sedimentary rocks of the Bulunkuole Complex, the Taxkorgan Fe ores are characterized by an assemblage of magnetite, pyrite and anhydrite. Due to the economic importance and unique mineral association, the age and genesis of these deposits were recently re-investigated (e.g., Chen, 2012; Yan et al., 2012a,b; Yang, 2013; Ren et al., 2013; Lin, 2015). Iron mineralization in the Taxkorgan terrane is generally considered to have formed in the Early Paleozoic, but the genesis of the deposits is variably attributed to be: (1) metamorphosed sedimentary-type or BIF (e.g., Chen et al., 2011, 2013; Feng et al., 2011; Ren et al., 2013; Qian et al., 2014; Qiao et al., 2015; Li et al., 2015b,c), and (2) submarine volcanogenic hydrothermal type (e.g., Chen, 2012, 2013; Yan et al., 2012a,b; Hu, 2014).

Zankan is the largest and most representative among the Taxkorgan Fe deposits. In this contribution, based on a compilation of published geological and geochemical data (including those by the authors), we discuss the genesis of the Zankan deposit.

2. Regional geology

On the southern margin of the Tarim Basin, the Pamir-West Kunlun-Altun Mountains (Pan and Wang, 1994; Xiao et al., 2000; Jiang et al., 2013; Wang et al., 2017a) connect with the East Kunlun (Zheng et al., 2016), Qinling (Chen and Santosh, 2014; Mao et al., 2014; Li et al., 2015a) and Dabie Shan (Wang et al., 2014, 2017b; Mi et al., 2015), and constitutes the Central China Orogenic Belt (CCOB; Chen et al., 2014). The CCOB was likely evolved from the northernmost Paleo-Tethys and took shape through the Early Mesozoic continental collision between

* Corresponding authors.
E-mail addresses: Tanghaoshu@163.com (H.-S. Tang), gigyjchen@126.com, yjchen@pku.edu.cn (Y.-J. Chen).

http://dx.doi.org/10.1016/j.oregeorev.2017.09.009
Received 30 August 2016; Received in revised form 11 September 2017; Accepted 12 September 2017
Available online 13 September 2017
0169-1368/

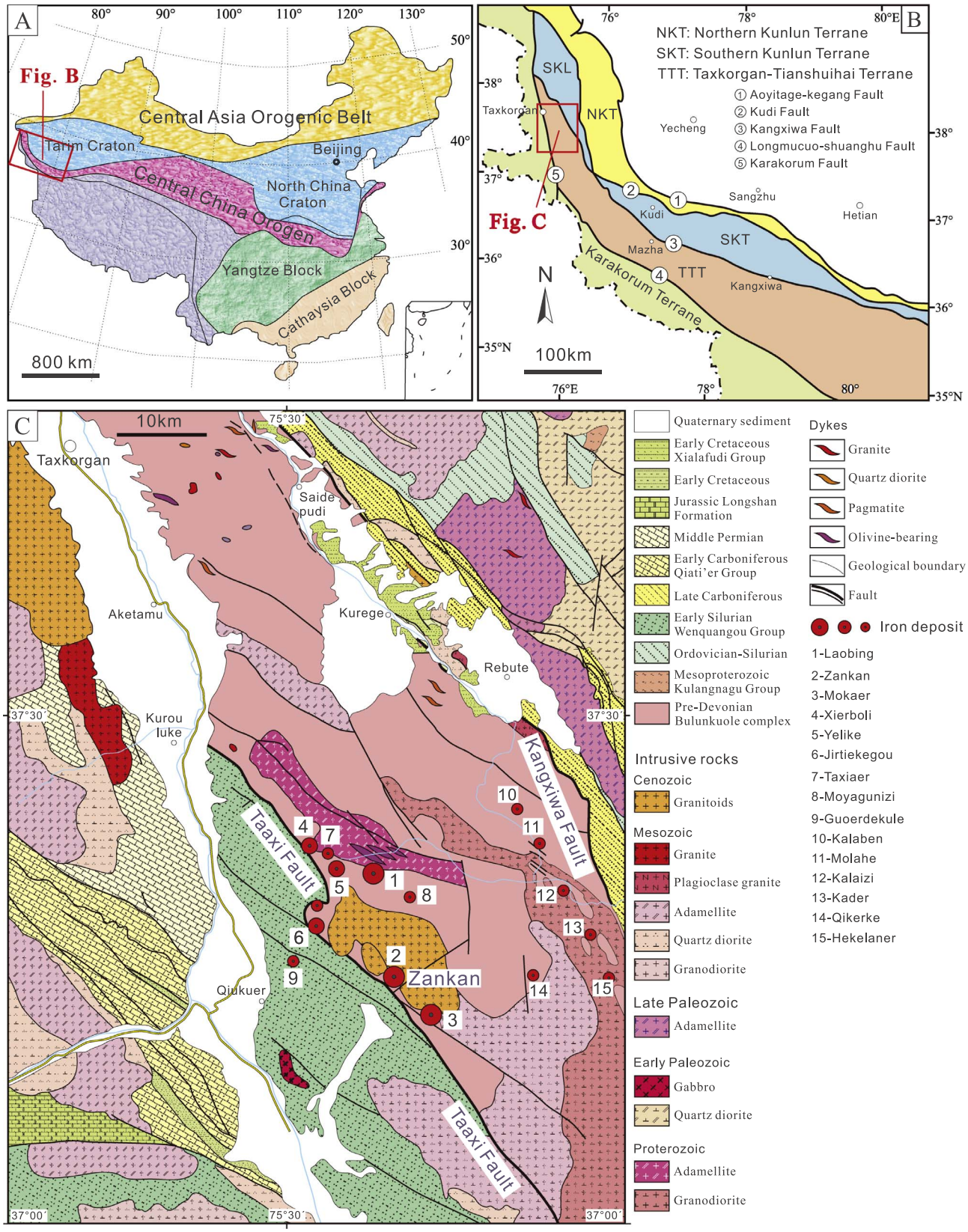

Fig. 1. (A) Tectonic subdivisions of China, showing the location of the West Kunlun Orogen; (B) tectonic subdivision of the West Kunlun Orogen, showing the location of the Taxkorgan Fe belt; (C) simplified geologic map of the Taxkorgan Fe belt. Modified after Ji et al. (2011) and Yan et al. (2012b).

the North China-Tarim plate and the Gondwana-derived tectonic blocks (Chen and Santosh, 2014; Zhou et al., 2014a,b, 2015, 2016; Li and Pirajno, 2017; Yang and Wang, 2017) (Fig. 1A).

The West Kunlun Orogen is bounded by the Aoyitage – Kegang Fault to the north and the Longmucuo-Shuanghu/Karakorum Fault to the south (Fig. 1B). It contains three tectonic units, namely (from north to

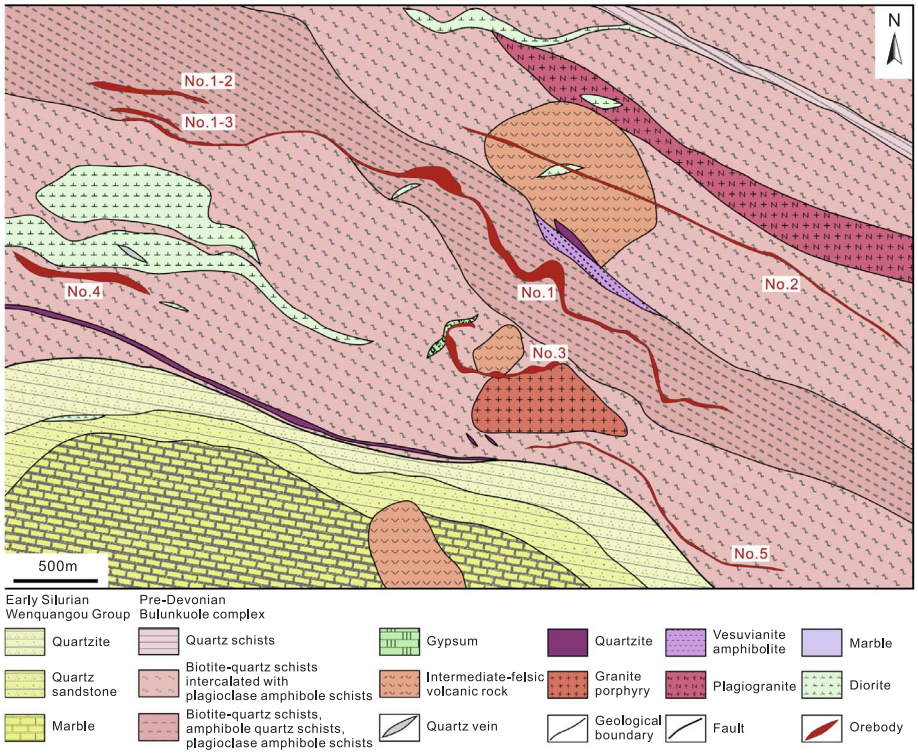

Fig. 2. Simplified geologic map of the Zankan Fe deposit.

south) the Northern Kunlun Terrane (NKT), the Southern Kunlun Terrane (SKT), and the Taxkorgan – Tianshuihai Terrane (TTT), with the Kudi and Kangxiwa faults defining their boundaries, respectively (Fig. 1B; Xiao et al., 2005; Yang et al., 2010).

The Taxkorgan terrane is located in the southernmost West Kunlun Orogen (Fig. 1B), bounded by the Kangxiwa Fault to the north and the Taaxi Fault (one fault of the Karakorum fault belt) to the south (Fig. 1C). Lithologies in the Taxkorgan terrrane are the pre-Devonian Bulunkuole Complex and Lower Cretaceous Xialafudi Group. The Bulunkuole Complex is metamorphosed to greenschist/amphibolite facies, and comprises biotite-plagioclase gneiss, plagioclase-amphibole gneiss-schist, biotite-quartz schist, sillimanite-garnet schist, magnetite quartzite, meta-siltstone and marble. Zircon U–Pb ages of these rocks range widely from *ca.* 500 to 2700 Ma (e.g., Sun et al., 2003; Zhang et al., 2007; Ji et al., 2011; Yan et al., 2012a,b; Qian et al., 2014). The Xialafudi Group unconformably overlies the Bulunkuole Complex, and consists of micritic limestone, conglomerate, sandstone, siltstone and shale deposited in a lacustrine environment. To the south and north, the Bulunkuole Complex and Xialafudi Group are separated from the Mesozoic granites and the Early Silurian Wenquangou Group by the Taaxi Fault, and from the Late Carboniferous clastic sediments by the Kangxiwa Fault, respectively (Fig. 1C). The Wenquangou Group comprises pelitic siltstone, mudstone, quartz sandstone, and minor conglomerate and carbonate intercalations. The Late Carboniferous unit comprises (silty)-mudstone, (micritic)-limestone and chert. The Taxkorgan terrane was intruded by the Proterozoic granodiorite and adamellite, followed by Mesozoic quartz diorite, adamellite and plagioclase granite, and Cenozoic syenogranite and syenite (Fig. 1C).

There are more than ten iron deposits in the Taxkorgan terrane, with the majority being hosted in the Bulunkuole Complex (Fig. 1C). Yan et al. (2012a,b) and Yang (2013) reported LA-ICP-MS zircon U–Pb ages of 526 ± 5.0 Ma and *ca.* 500 Ma for the Laobing and Ziluoyi deposits, respectively. Lin (2015) and Dong et al. (2016) reported LA-ICP-MS zircon U–Pb ages of 527.4 ± 9.0 Ma to 536.8 ± 3.4 Ma for the volcanic rocks that host the Zankan Fe ores. Therefore, the Fe mineralization in the Taxkorgan terrane mainly occurred in the Cambrian, coeval with the development of an Andean-type magmatic arc (540–435 Ma) in the West Kunlun Orogen (Xu et al., 1994; Pan and Bian, 1996; Mattern and Schneider, 2000; Xiao et al., 2005; Liao et al., 2010; Jia et al., 2013; Liu et al., 2014; Cao et al., 2016).

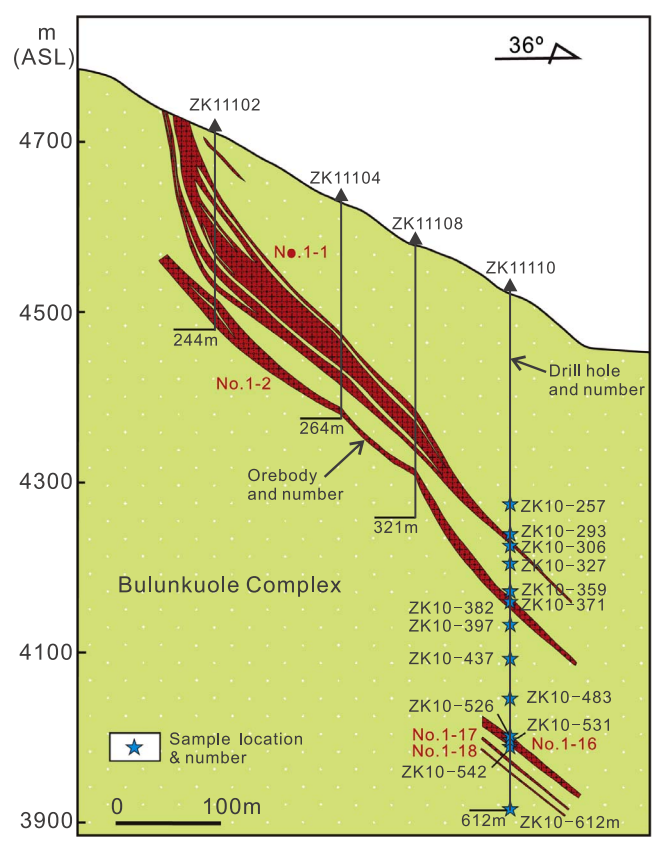

Fig. 3. Geological section of No. 111 prospecting line at the Zankan Fe deposit.

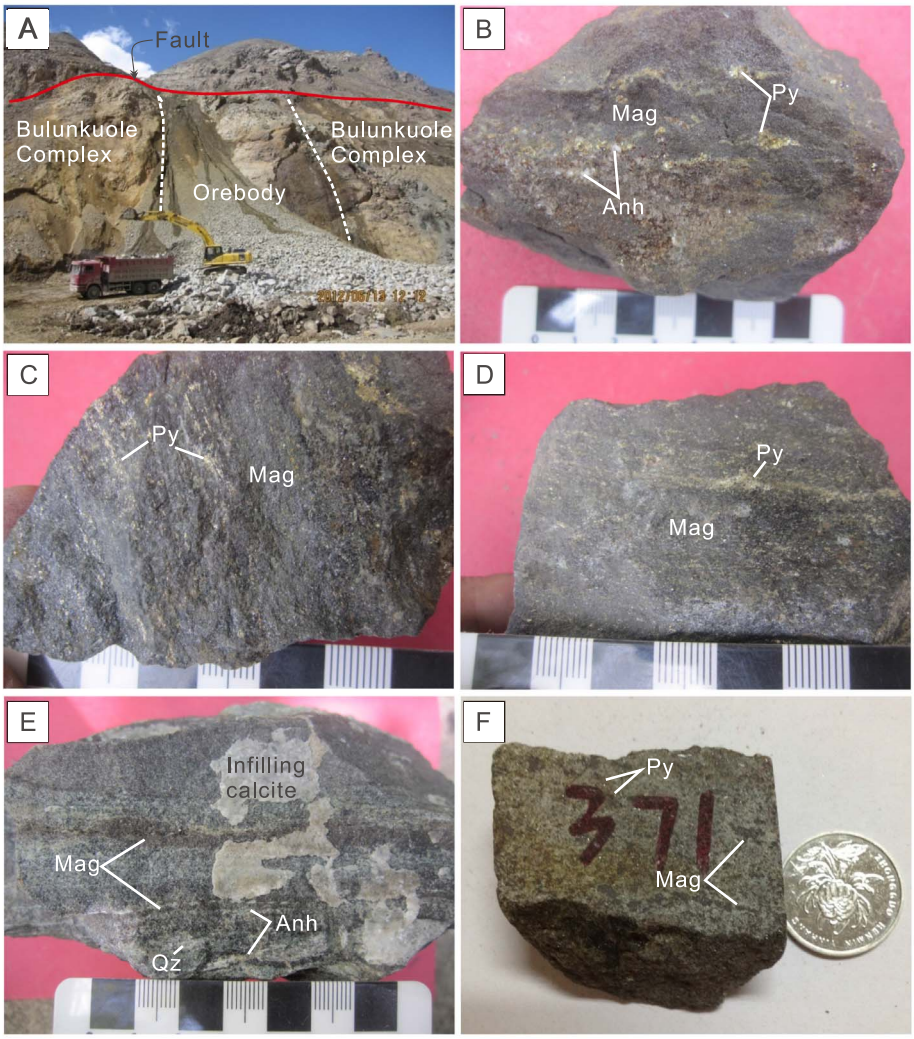

Fig. 4. Photos of ores from the Zankan Fe deposit. (A) Stratiform orebodies in the Bulunkuole Complex; (B) Massive ores containing magnetite, pyrite and anhydrite; (C), (D) Massive ores containing magnetite and laminated pyrite; (E) Banded ores containing magnetite, quartz and anhydrite; (F) Disseminated ores containing magnetite and pyrite. Abbreviations: Mag, magnetite; Py, pyrite; Qz, quartz; Anh, anhydrite.

3. Deposit geology

The Zankan iron deposit is located in the northern part of the Taxkorgan terrane (Fig. 1C), with a proven reserve of 146 Mt (million tonnes) Fe (grade: 28.3–58.8%) and an inferred resource of 180 Mt Fe (Dong et al., 2011; Feng et al., 2011). Major lithostratigraphic units at Zankan are the Bulunkuole Complex and Wenquangou Group (Fig. 2). The orebodies are hosted in the Bulunkuole Complex, and spatially associated with the metamorphosed continental arc dacite and andesite (Lin, 2015; Dong et al., 2016). Two volcanic rock samples from the hanging wall and the contact of the orebody and footwall rocks yielded LA-ICP-MS zircon U–Pb ages of 536.4 ± 4.0 Ma and 536.8 ± 3.4 Ma, respectively (Dong et al., 2016). Lin (2015) reported zircon U–Pb ages of 533 ± 10 Ma and 527.4 ± 9.0 Ma for the sub-volcanic rocks that intruded the footwall of the Fe orebodies. Phanerozoic diorite, granite porphyry and plagiogranite occur in the mining area (Fig. 2).

There are five orebodies at Zankan. The No. 1 orebody is the largest and accounts for 72.01% of the total reserve. It is 2493 m long, 10.40–21.12 m thick, and trends 30–40° (NE-dipping at 27–70°). The No. 3 orebody is the second largest, > 1000 m long, 8.8–14.0 m thick and trends 19–41° (NE-dipping at 6 − 57°). The other three orebodies are generally > 400 m long and about 10 m thick. The Zankan Fe orebodies appear are stratiform or stratabound (Figs. 2, 3, 4A).

The ores have similar ore-mineral association of magnetite, pyrite, chalcopyrite and pyrrhotite, but are classified by local geologists into three types (massive (Fig. 4B − D), banded (Fig. 4E) and disseminated (Fig. 4F)) according to their different proportions of these minerals and occurrence of magnetite. Gangue minerals include quartz, anhydrite, plagioclase, hornblende, biotite, muscovite and calcite, and minor sphene and apatite (Zhou et al., 2017). Magnetite is euhedral to anhedral (0.06–0.5 mm long) (Fig. 5) and is locally replaced by pyrite and pyrrhotite (Fig. 5B and C). Pyrite occurs as laminations and disseminations (Fig. 4C, D and F) and coexists with magnetite and anhydrite (Fig. 4B and E). The pyrite is subhedral to anhedral, and is generally 0.06 to 0.9 mm long (Fig. 5C − E). Chalcopyrite is anhedral and replaced pyrite and pyrrhotite (Fig. 5B and C). Pyrrhotite is subhedral to anhedral and locally coexists with pyrite and magnetite (Fig. 5D).

4. Analytical methods

4.1. Major and trace element analysis

Major elements analysis was conducted at the ALS Chemex (Guangzhou) Co. Ltd. For the major elements, SiO_2, TiO_2, Al_2O_3, $Fe_2O_3^T$, MgO, MnO, CaO, Na_2O, K_2O and P_2O_5 were determined using a PANalytical Axios X-ray Fluorescence spectrometer (XRF) on fused glass beads, and the FeO was determined by wet chemical method. The analytical uncertainty is below 5%. Trace elements (including rare earth elements) were determined using inductively coupled plasma mass spectrometer (ICP-MS) at the Guiyang Institute of Geochemistry, Chinese Academy of Sciences (GIGCAS), with an analytical precision better than 10% RSD. The Standards OU-6, AMH-1 and GBPG-1 were

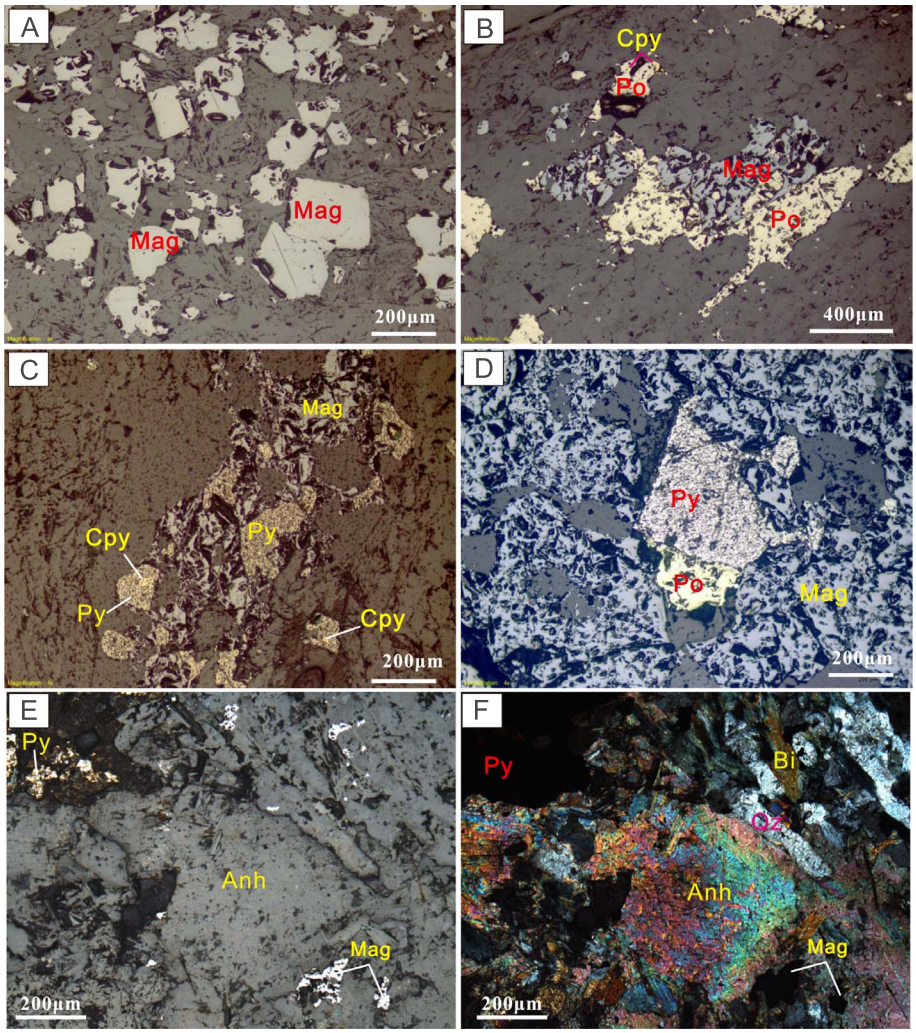

Fig. 5. Reflected-light (A–E) and cross-polarized light (F) photomicrographs of the ore minerals at Zankan. (A) Subhedral to euhedral magnetite grains; (B) Anhedral magnetite replaced by pyrrhotite, followed by chalcopyrite; (C) Anhedral magnetite replaced by pyrite, followed by chalcopyrite; (D) Anhedral magnetite coexists with subhedral pyrite and pyrrhotite; (E) Anhedral magnetite coexists with subhedral pyrite; (F) Anhedral magnetite coexists with anhydrite. Abbreviations: Mag, magnetite; Py, pyrite; Cpy, chalcopyrite; Po, pyrrhotite; Qz, quartz; Ms, muscovite; Bi, biotite; Anh, anhydrite.

used as reference materials. The procedure for the trace element analysis was as described by Qi and Gregoire (2000)

4.2. Sulfur isotopes

Sulfur isotopes for sulfides were analyzed by EA-IRMS (Elemental Analysis-Isotope Ratio Mass Spectrometry), using a EuroVector EA3000 element analyzer and a GV IsoPrime spectrometer at the GIGCAS. Mineral separates were handpicked from the crushed and washed sample fragments under a binocular microscope to achieve > 99% purity. The powdered sulfide separates were packed in tinfoil, and converted to SO_2 for isotope analysis by burning in the reactor under a constant temperature of about 1000 °C using a stream of purified oxygen. The sulfur dioxide was then carried by helium into the mass spectrometer. Sulfur isotopic data are reported in per mil (‰) relative to the Canyon Diablo Troilite standard (CDT) and calibrated by international standard samples GBW-4414 (Ag_2S, $\delta^{34}S = -0.07$‰) and GBW-4415 ($\delta^{34}S = 22.15$‰). Analytical precision is better than ± 0.2‰.

Sulfur isotopes for whole-rock samples were analyzed by a MAT 253 mass spectrometer in the Analytical Laboratory of Beijing Research Institute of Uranium Geology. Barium sulfate was extracted from the samples (200 mesh) by using sodium carbonate-zinc oxide half melting method. Subsequently, a composite sample of barium sulfate, vanadium pentoxide and quartz sand (with a weight ratio of 1:3.5:3.5) was put into a vacuum system and heated to 980 °C to obtain SO_2. The SO_2 was analyzed on a mass spectrometer. Sulfur isotope data were reported in per mil (‰) relative to the Canyon Diablo Troilite standard (CDT). Analytical precision is better than ± 0.2‰.

5. Results

5.1. Major elements of the Fe ores

Major element compositions of the Zankan Fe ore samples are listed in Table 1. The ore samples contain variable contents of hornblende, biotite, muscovite, calcite and anhydrite as shown by their LOI values up to 9.46 wt%. Their major oxide contents were recalculated to 100% as volatile-free. The ore samples are characterized by high $Fe_2O_3^T$ (35.6–93.9 wt%, average 64.6 wt%) and relatively low SiO_2 (1.85–47.8 wt%, average 20.0 wt%), with minor but variable Al_2O_3 (0.16–5.26 wt%), MgO (0.43–7.60 wt%), CaO (0.45–16.9 wt%) and P_2O_5 (0.04–2.34 wt%). Contents of K_2O (< 0.01–2.46 wt%), Na_2O (< 0.01–1.36 wt%), TiO_2 (0.04–0.41 wt%), and MnO (0.09–1.76 wt%) are all very low. Except for four samples, most of the Zankan Fe ore samples have $Fe^{3+}/(Fe^{3+}+Fe^{2+})$ ratios of 0.60 to 0.73, resembling the magnetite theoretical value (0.67), indicating that magnetite is the main ore mineral. Thus, the Zankan Fe ores contain mainly magnetite and quartz, with a strongly negative $Fe_2O_3^T$ vs. SiO_2 correlation (Fig. 6A). Compared to the Canadian Algoma-type (average: SiO_2 = 48.9 wt%; $Fe_2O_3^T$ = 39.7 wt%) and Lake Superior-type (average: SiO_2 = 47.1 wt%; $Fe_2O_3^T$ = 40.3 wt%) BIFs (Gross and McLeod, 1980), the Zankan Fe ores have lower SiO_2 and higher $Fe_2O_3^T$ contents.

Table 1
Contents of major, trace and rare earth elements of the Zankan Fe ores.

Sample no.	A1-20	PM6-2	PM6-1	A 3-1	10-371	10-531	PM6-4	10-359	10-526	A1-02	PM8-1	PM10-1	10-306	10-382
description	B	M	M	M	D	D	M	M	M	B	M	M	M	D
(%)														
SiO_2	21.2	34.8	1.67	2.61	39.5	10.6	24.23	21.2	2.10	13.7	24.5	10.9	41.6	46.3
Al_2O_3	3.25	5.23	0.38	0.29	2.71	0.16	3.52	1.22	0.15	0.46	1.71	0.56	4.58	4.95
$Fe_2O_3^T$	40.9	46.1	72.0	93.7	49.2	85.3	48.3	61.8	80.5	56.0	68.4	77.8	30.0	34.5
MgO	4.69	2.51	5.59	0.96	4.17	0.43	7.21	6.64	2.96	4.39	3.43	2.70	3.94	3.94
CaO	14.8	6.87	10.45	1.56	0.45	2.34	9.54	8.60	6.42	15.1	1.26	6.41	11.0	3.30
Na_2O	0.30	0.85	< 0.01	0.03	0.14	0.13	0.16	0.09	< 0.01	< 0.01	0.22	0.08	1.04	1.32
K_2O	0.51	2.45	0.04	0.01	0.82	< 0.01	0.72	0.52	< 0.01	0.05	0.57	0.01	1.85	1.54
MnO	0.79	0.42	0.28	0.09	1.74	0.20	0.84	1.01	0.67	0.72	0.27	0.19	0.94	0.61
P_2O_5	0.78	0.06	0.04	0.24	0.11	1.18	0.15	0.18	0.72	2.18	0.11	1.94	0.14	0.22
TiO_2	0.36	0.22	0.04	0.33	0.11	0.12	0.19	0.06	0.26	0.37	0.09	0.35	0.16	0.22
LOI	8.95	−0.28	9.46	−1.80	1.72	−0.34	5.12	−2.22	−0.28	4.31	−0.83	−0.94	4.29	2.34
Total	96.53	99.23	99.95	98.02	100.67	100.12	99.98	99.10	93.50	97.28	99.73	100	99.54	99.24
(ppm)														
V	1016	95.0	3730	6270	71.0	2630	103	455	5390	1377	57.0	4660	96.0	84.0
Co	25.4	83.0	204	31.0	137	115	138	49.0	51.0	27.9	123	100	98.0	175
Ni	26.8	< 1	62.0	14.0	10.0	119	16.0	< 1	201	27.4	< 1	46.0	20.0	12.0
Cu	5.99	7.00	147	< 1	331	62.0	1010	5.00	12.0	3.07	61.0	181	482	196
Zn	21.2	36.0	57.0	15.0	14.0	35.0	14.0	29.0	26.0	33.7	31.0	23.0	36.0	18.0
As	13.0	< 5	24.0	5.00	< 5	< 5	15.0	< 5	6.00	12.9	6.00	18.0	7.00	< 5
Mo	1.34	16.0	2.00	< 1	12.0	< 1	50.0	3.00	< 1	0.69	172	< 1	9.00	< 1
Pb	2.80	16.0	24.0	6.00	5.00	10.0	9.00	8.00	9.00	0.53	10.0	15.0	15.0	2.00
Cr	50.6	30.0	10.0	< 10	10.0	< 10	20.0	< 10	< 10	63.2	20.0	< 10	20.0	30.0
Ga	28.7	3.30	28.4	49.6	6.90	41.9	6.50	13.5	43.1	32.9	6.40	27.1	11.5	9.60
Rb	16.0	60.6	0.90	0.50	26.3	0.80	19.1	42.5	2.10	1.88	47.3	0.70	49.6	54.5
Sr	48.2	98.1	45.1	5.70	4.40	112	67.5	22.2	102	33.5	54.0	14.7	149	79.4
Y	80.3	15.1	97.1	14.8	15.0	129	21.0	46.7	97.9	166	7.70	37.6	30.7	16.6
Zr	25.7	83.0	4.00	6.00	31.0	3.00	45.0	16.0	3.00	6.53	34.0	3.00	71.0	71.0
Nb	2.53	5.30	0.40	1.60	2.10	4.20	2.80	4.00	0.80	1.05	2.80	0.50	3.10	5.00
Cs	1.20	2.79	0.20	0.15	0.64	0.05	1.04	3.77	0.39	0.29	3.01	0.24	1.25	2.19
Ba	97.1	1770	5.50	2.50	423	27.2	252	275	189	6.57	1885	12.5	1815	2240
La	30.7	41.5	46.7	6.80	15.3	108	234	334	238	158	219	125	554	89.9
Ce	72.1	55.8	113	15.7	21.7	250	350	576	526	148	292	277	736	127
Pr	9.50	3.99	11.8	1.63	1.74	26.9	26.1	50.1	57.4	48.8	20.0	26.6	53.7	10.1
Nd	40.5	11.2	48.0	6.70	5.80	103	70.4	150	217	198	48.9	94.8	141	28.7
Sm	10.1	1.61	11.0	1.62	1.36	20.0	9.86	19.2	39.3	38.6	5.14	14.4	17.4	3.45
Eu	1.38	1.06	2.10	0.15	0.54	1.39	4.39	4.60	2.41	3.39	3.50	1.67	6.89	1.15
Gd	8.86	1.61	13.2	2.25	2.33	19.4	5.48	13.4	27.8	25.9	2.97	9.96	11.6	2.82
Tb	2.08	0.31	2.22	0.35	0.45	3.14	0.70	1.68	3.47	5.23	0.36	1.18	1.35	0.43
Dy	14.3	2.42	14.2	2.33	2.83	19.9	4.33	8.79	19.1	30.8	1.92	6.44	6.49	2.89
Ho	3.37	0.56	3.35	0.50	0.53	4.58	0.79	1.75	3.65	6.89	0.31	1.26	1.16	0.57
Er	9.32	1.98	10.3	1.37	1.39	13.7	2.25	4.72	9.97	18.5	0.90	3.54	3.07	1.76
Tm	1.30	0.36	1.74	0.28	0.22	2.26	0.40	0.71	1.61	2.45	0.17	0.58	0.49	0.32
Yb	8.44	2.01	10.7	1.17	1.20	13.8	1.90	4.25	9.24	15.7	0.91	3.37	3.14	1.76
Lu	1.34	0.25	1.80	0.22	0.14	2.51	0.28	0.69	1.42	2.33	0.13	0.59	0.49	0.26
Hf	1.04	2.00	< 0.2	0.20	0.80	< 0.2	1.10	0.40	< 0.2	0.82	0.90	< 0.2	1.80	1.80
Ta	0.19	0.50	0.20	0.30	0.20	0.20	0.40	0.20	0.10	0.21	0.30	0.10	0.30	0.40
W	127	510	107	150	499	435	392	324	145	60.8	460	354	302	988
Th	4.19	2.19	3.29	3.66	1.49	3.23	2.55	2.55	2.70	17.3	1.62	2.95	4.37	4.06
U	1.70	3.58	9.44	1.60	10.2	2.57	15.9	28.1	1.92	1.85	20.1	3.42	28.3	2.80
REY	294	140	387	55.9	70.5	717	732	1216	1254	868	604	604	1567	287
La/Ce	0.43	0.74	0.41	0.43	0.71	0.43	0.67	0.58	0.45	1.07	0.75	0.45	0.75	0.71
Y/Ho	23.8	27.0	29.0	29.6	28.3	28.2	26.6	26.7	26.8	24.1	24.8	29.8	26.5	29.1
$(Nd/Yb)_{PASS}$	0.40	0.46	0.37	0.48	0.40	0.62	3.08	2.94	1.95	1.05	4.47	2.34	3.74	1.36
$(Sm/Yb)_{PASS}$	0.61	0.41	0.52	0.70	0.58	0.73	2.64	2.29	2.16	1.25	2.87	2.17	2.82	1.00
$(La/La^*)_{PASS}$	0.96	1.56	1.05	1.12	1.61	0.92	1.30	1.07	0.93	0.85	1.47	0.95	1.46	1.37
$(Eu/Eu^*)_{PASS}$	0.61	3.01	0.85	0.40	1.40	0.34	2.73	1.41	0.36	0.46	4.19	0.69	2.38	1.78
$(Ce/Ce^*)_{PASS}$	0.96	0.91	1.11	1.09	0.91	1.07	0.97	1.00	1.04	0.39	0.92	1.11	0.90	0.91
FeO		14.8	17.5	26.5	40.7	24.6	15.0	20.0			21.1	28.0	12.2	22.6
XFe^{3+}		0.64	0.73	0.69	0.27	0.66	0.66	0.26			0.66	0.60	0.84	0.49

B = banded, D = dissemination, M = massive. $Fe_2O_3^T$, total Fe expressed as Fe_2O_3; LOI, Loss on ignition, stands for the pre-ignition weight minus post-ignition weight, and negative LOI values result from oxidation of low valence elements and gain of oxygen during ignition; XFe^{3+}, $Fe^{3+}/(Fe^{2+} + Fe^{3+})$.

5.2. Trace and rare earth elements

Trace and rare earth element (REE) concentrations of the Zankan ore samples are presented in Table 1. Yttrium shows similar chemical behavior to REEs, and is therefore inserted between Dy and Ho based on its ionic radius (Bau et al., 1996). The REY (REE + Y) of the ore samples are normalized to the post-Archean Australian shale (PAAS, McLennan, 1989). Lanthanum and Y anomalies are defined as: $La/La^*_{PAAS} = La_{PAAS}/(3Pr_{PAAS} - 2Nd_{PAAS})$, and Y anomalies assessed using the Y/Ho ratio (higher or lower than 26), respectively (Bolhar et al., 2004). Europium and Ce anomalies are defined as $Eu/Eu^*_{PAAS} = Eu_{PAAS}/(0.67Sm_{PAAS} + 0.33Tb_{PAAS})$, and $Ce/Ce^*_{PASS} = Ce_{PASS}/(0.5La_{PASS} + 0.5Pr_{PASS})$, respectively (Bau and Dulski, 1996). The LREE/HREE and MREE/HREE fractionations are expressed as $(Nd/Yb)_{PASS}$ and $(Sm/Yb)_{PASS}$, respectively, owing to the La and Ce anomalies in seawater.

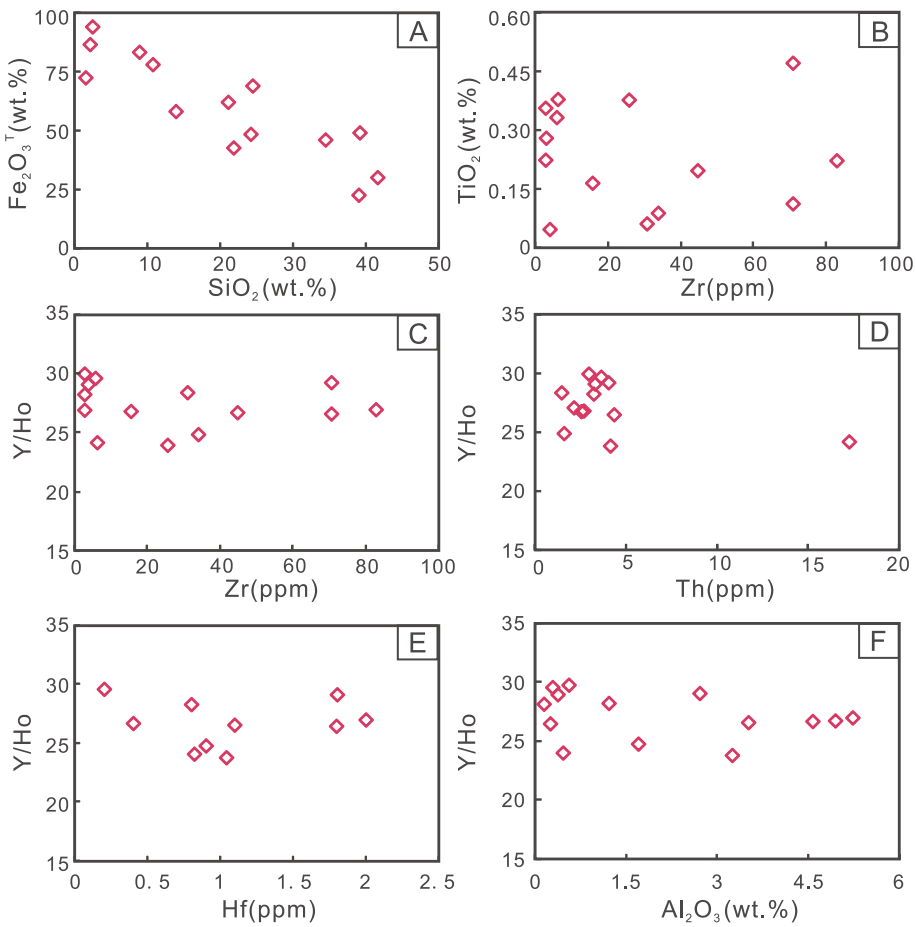

Fig. 6. Binary diagrams for the Zankan Fe ores.

The analyzed samples can be divided into three groups according to their REY geochemistry (Fig. 7). Group 1 (samples A1-20, PM6-2, A3-1, PM6-1, 10-371 and 10-531) (Table 1; Fig. 7) shows relatively low ΣREY (56–717 ppm), and LREE/HREE (Nd/Yb_{PAAS} = 0.37–0.62) and MREE/HREE ratios (Sm/Yb_{PAAS} = 0.41–0.73). Group 2 (samples PM6-4, 10-359, 10-526, A1-02, PM8-1, PM10-1 and 10-306) is characterized by relatively higher ΣREY (604–1567 ppm), LREE and MREE enrichment (Nd/Yb_{PAAS} = 1.05–4.47, Sm/Yb_{PAAS} = 1.25–2.87). Group 3 (sample 10-382) shows LREE enrichment (Nd/Yb_{PAAS} = 1.36) but lacks MREE enrichment (Sm/Yb_{PAAS} = 1). Most samples of these three groups show positive La ($La/La*_{PAAS}$ = 0.85–1.61, average 1.19) and Y (Y/Ho = 24–30, average 27) anomalies. Eight (out of 14) samples exhibit negative Ce anomalies ($Ce/Ce*_{PAAS}$ = 0.39–0.97), whereas the other six show no or weak positive Ce anomalies ($Ce/Ce*_{PAAS}$ = 1.0–1.11). Half of the samples exhibit negative Eu anomalies ($Eu/Eu*_{PAAS}$ = 0.34–0.85), whereas the other half show positive Eu anomalies ($Eu/Eu*_{PAAS}$ = 1.4–4.19) (Fig. 8).

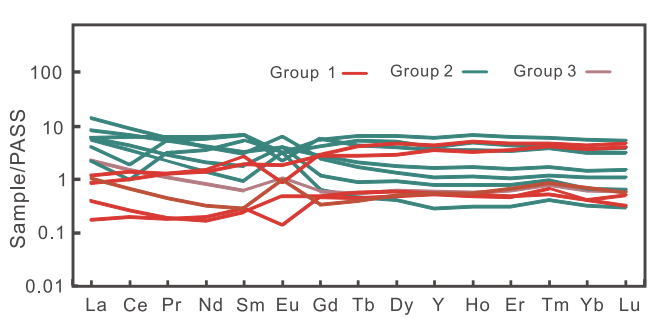

Fig. 7. PASS-normalized REY pattern of the Zankan Fe ores (PASS value from McLennan (1989)).

5.3. Sulfur isotope compositions

Sulfur isotopes of the Zankan ores and host rocks are listed in Table 2, and isotope variation of the drill core ZK11110 is shown in Fig. 9. Pyrite grains selected from different magnetite ores (disseminated and laminated) (Fig. 4C, D, F), indicating that pyrite and magnetite were formed simultaneously. The $\delta^{34}S$ values of pyrite grains from the ores range from 3.2 − 32.8‰, with an average of 23.0‰ (Table 2 and Fig. 10A). The pyrite, pyrrhotite and host rocks from the Bulunkuole Complex have $\delta^{34}S$ values of 19.1–31.7‰, 28.7–32.0‰, and 2.6–30.2‰, with averages of 23.6‰, 30.4‰, and 16.1‰, respectively (Table 2; Fig. 10B). The $\delta^{34}S$ values of Zankan ores are similar to those of the Bulunkuole Complex, probably reflecting a *syn*-depositional metallogenesis and/or a sulfur contribution from the latter. The $\delta^{34}S$ values for the drill core ZK11110 (from top to bottom) vary in the range of 2.6‰ to 32.0‰ (Fig. 9).

6. Discussion

6.1. Ore deposit type

The Zankan orebodies are hosted in metamorphosed volcanic-sedimentary rocks (Fig. 2) and display sedimentary features. The orebodies are stratiform or form lenses (Fig. 2), and the ores are laminated, banded or massive (Fig. 4C–E). Major minerals are Fe-oxides (magnetite), sulfides (pyrite, chalcopyrite and pyrrhotite), and sulfates (barite, anhydrite and gypsum), together with varying contents of quartz (Fig. 4B–E and 5). Microscope observations show that anhydrite and barite coexist with magnetite (Fig. 5F), implying their co-precipitation

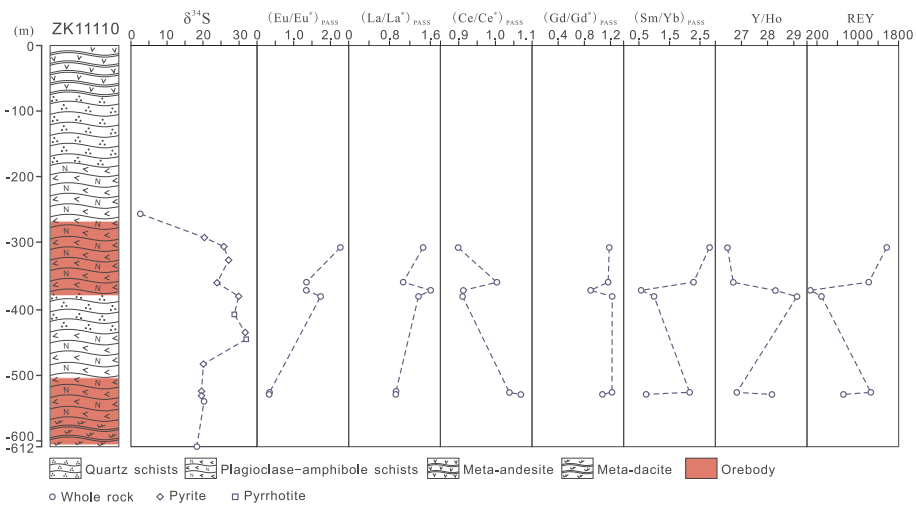

Fig. 8. Plot of Eu/Eu*$_{PAAS}$ vs. Ce/Ce*$_{PAAS}$ for the Zankan Fe ores.

in the same hydrothermal system. Nijman et al. (1998) suggested that most sulfates, such as anhydrite and barite, precipitated originally from hydrothermal emanations analogous to white smokers, and thus we consider that the oxide-sulfide-sulfate assemblages of the Zankan deposit were precipitated from seafloor hydrothermal systems.

The $\delta^{18}O$ values of the Zankan magnetite fall inside a narrow range of 3.9–7.8‰ (Yan et al., 2012a), and overlap with those of primary sedimentary magnetite (1.3–6.8‰; Li and Yang, 1983), indicating a sedimentary origin of the Zankan magnetite. The $\delta^{18}O$ values are also comparable to those of the Fe deposits in the West Kunlun Orogen, such as Zuokeben (3.3–4.6‰; Chen, 2013) and Laobing (3.3–7.2‰; Yan et al., 2012b), in which the ores were interpreted to have deposited by submarine volcanic-sedimentary processes. The magnetite trace element data from Zankan indicate that the magnetite grains have high contents of Ti, Al, and V (Zhou et al., 2017), which is generally considered to be indicative of relatively reduced seafloor hydrothermal systems (Carew, 2004). The Fe isotope fractionation between pyrite and magnetite ($\triangle\delta^{57}Fe_{py\text{-}mag}$) ranges 0.2–1.1‰, implying a high-temperature precipitation environment (≥236 °C) (Zhou et al., 2017). These features suggest that the Zankan Fe deposit was likely formed in a seafloor hydrothermal system (Zhou et al., 2017).

Table 2
^{34}S (‰) values of the Fe ores and host rocks at Zankan deposit.

No.	Sample geology	Sample no.	Mineral/rock	$\delta^{34}S$
	Ore			
1	Massive magnetite ore	10-293	Pyrite	20.4
2	Massive magnetite ore	10-306	Pyrite	25.8
3	Disseminated magnetite	10-327	Pyrite	27.1
4	Massive magnetite ore	10-359	Pyrite	23.9
5	Disseminated magnetite	10-382	Pyrite	29.9
6	Massive magnetite ore	10-526	Pyrite	19.6
7	Disseminated magnetite	10-531	Pyrite	19.6
8	Massive magnetite ore	PM11-2	Pyrite	21.2
9	Massive magnetite ore	PM6-2	Pyrite	29.5
10	Massive magnetite ore	PM6-3	Pyrite	32.8
11	Massive magnetite ore	PM6-4	Pyrite	32.7
12	Massive magnetite ore	PM3-1	Pyrite	20.5
13	Massive magnetite ore	PM10-1	Pyrite	19.9
14	Massive magnetite ore	PM10-2	Pyrite	17.5
	Average	**N = 14**		**24.3**
15	Massive magnetite ore	PM11-4	Pyrite	3.2
	Bulunkuole Complex			
16	Biotite-quartz schist	10-397	Pyrrhotite	28.7
17	Amphibole-quartz schist	10-437	Pyrite	31.7
18	Amphibole-quartz schist	10-437	Pyrrhotite	32.0
19	Biotite-quartz schist	10-483	Pyrite	20.1
20	Amphibole-quartz schist	10-542	Whole rock	20.3
21	Biotite-quartz schist	PM4-1	Pyrite	19.1
22	Metamorphosed and altered dacite	10-612	Whole rock	18.3
23	Metamorphosed and strongly-altered dacite	A0-13	Whole rock	28.3
24	Metamorphosed and altered dacite	A0-5	Whole rock	15.4
25	Metamorphosed and strongly-altered dacite	A0-1	Whole rock	30.2
	Average	**N = 10**		**24.4**
26	Amphibole-quartz schist	10-257	Whole rock	2.6
27	Metamorphosed dacite	A0-11	Whole rock	6.8
28	Metamorphosed dacite	A0-17	Whole rock	6.9
	Average	**N = 3**		**5.4**

6.2. Source of the ore-forming fluids

Four of the Zankan ore samples (PM6-2, PM6-1, A3-1 and 10-371) show LREE and MREE depletions (relative to HREE), and positive La and Y anomalies (Table 1), which resemble typical modern seawater (Bolhar et al., 2004). Half of the ore samples show positive Eu anomalies (Eu/Eu* = 1.14–4.19; Fig. 8), which could not have been inherited from seawater because of their absence in seawater (e.g., Zhang and Nozaki, 1996; Alibo and Nozaki, 1999; Freslon et al., 2011) or in hydrogenetic marine sediments (e.g., Bau et al., 1996; Surya Prakash et al., 2012). In modern marine environments, pronounced positive Eu anomalies are only observed in high-temperature (> 250 °C) hydrothermal systems at mid-ocean ridges and back-arc spreading centers, where alteration of seafloor basalts and other mafic rocks contributes REY, Fe^{2+} and Mn^{2+} to the hydrothermal systems (Bau and Dulski, 1996, 1999). The Fe isotope fractionation between

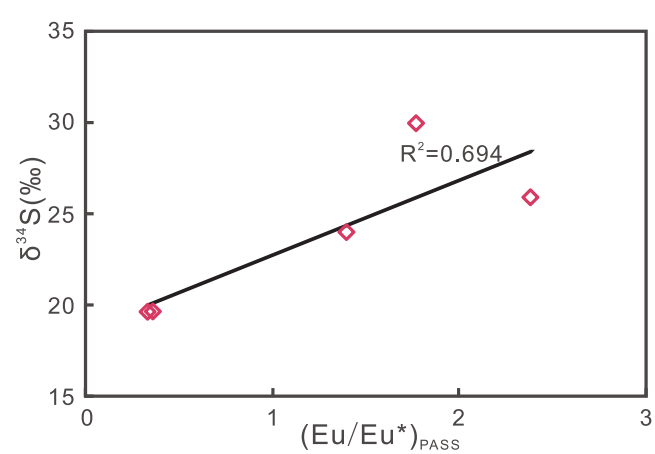

Fig. 9. $\delta^{34}S$ values and trace element variation of the drill core ZK11110.

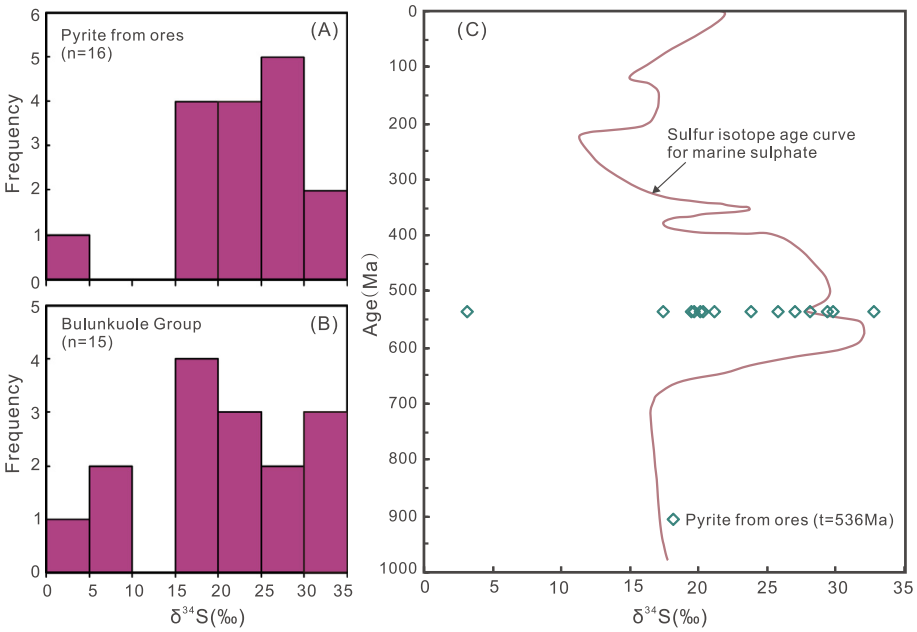

Fig. 10. Histograms of $\delta^{34}S$ values of the Fe ores (A) and host rocks (B) from the Zankan deposit; and plot of the Zankan deposit (C) on temporal $\delta^{34}S$ variation (Holser, 1977).

pyrite and magnetite suggests that the Zankan deposit may have formed under high temperature (≥236 °C) (Zhou et al., 2017), which further implies the presence of high-temperature hydrothermal fluids in the Zankan Fe metallogenesis. In addition, the observed LREE/HREE enrichment in seven Zankan ore samples (Nd/Yb_{PAAS} = 1.05–4.47; Table 1) is also indicative of a hydrothermal source for the metals (Hongo and Nozaki, 2001). The remaining seven samples that display negative Eu anomalies ($Eu/Eu*_{PAAS}$ = 0.34–0.85, Fig. 8) possibly imply continental crust contamination and/or sediment contribution via subduction-related dehydration (Oksuz, 2011).

Our study shows that the Fe at Zankan was mainly derived from hydrothermal fluids and seawater (hydrogenous). This trend is observed for the major oxides and trace elements of the studied ores. The presence of both hydrothermal and hydrogenous metallogenic inputs of the Zankan deposit is supported by the Al_2O_3 vs. SiO_2 (Fig. 11A; Wonder et al., 1988) and (As + Cu + Mo + Pb + V + Zn) vs. (Co + Ni) (Fig. 11B; Nicholson, 1992) discrimination diagrams. According to Nath et al. (1997), hydrothermal crusts have a much higher La/Ce ratio (~2.8) than those of hydrogenous Fe-Mn crusts (~0.25), and the La/Ce ratios of the Zankan deposit (0.41 to 1.07; average 0.61) lie between these two end-members (Table 1). Eight (out of 14) ore samples exhibit negative Ce anomalies ($Ce/Ce*_{PAAS}$ = 0.39–0.97; Fig. 8) and suggest a hydrothermal contribution, whereas the rest with no or weak positive Ce anomalies ($Ce/Ce*_{PAAS}$ = 1.0–1.11) suggest a hydrogenous contribution (Oksuz, 2011; Zarasvandi et al., 2013).

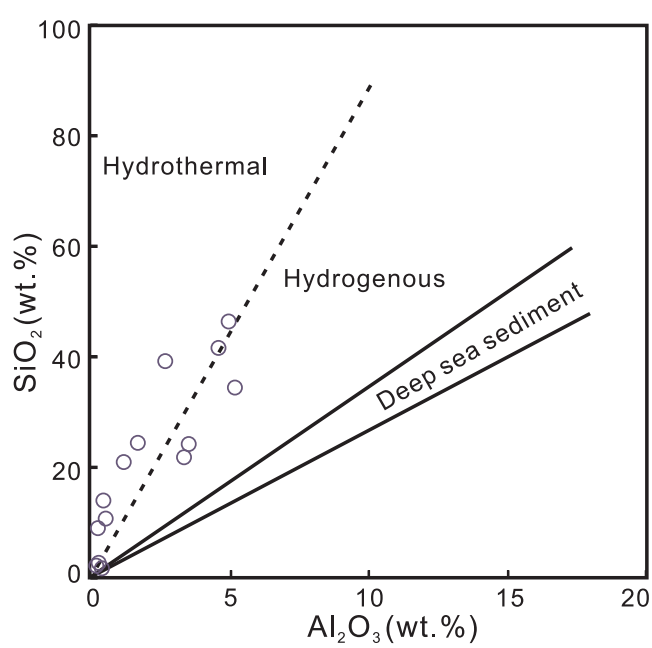

Fig. 11. Plots of Al_2O_3 vs. SiO_2 (A; Wonder et al., 1988) and (As + Cu + Mo + Pb + V + Zn) vs. (Ni + Co) (B; Nicholson, 1992) for the Zankan Fe ores.

The wide $\delta^{34}S$ range of the Zankan ores (3.2‰ to 32.8‰) (Table 2; Fig. 10A) suggests that multiple sulfur sources may have existed. It is generally accepted that near-zero $\delta^{34}S$ values commonly indicate a magmatic source, and highly positive $\delta^{34}S$ values show sedimentary sulfate contributions (Hoefs, 1997). The $\delta^{34}S$ values at Zankan are comparable to the nearby Laobing Fe deposit (5.2 to 19.7‰), which was interpreted to have been related to a volcanogenic sedimentary system (Yan et al., 2012a,b). Thus, the low $\delta^{34}S$ (3.2‰) for Zankan pyrite may have been volcanic-related, whereas the high $\delta^{34}S$ ones (17.5–32.8‰) were close to the anhydrite (29–37.1‰) co-precipitated with the Laobing magnetite (Yan et al., 2012a). Furthermore, the high $\delta^{34}S$ values of some Zankan pyrite are comparable to those of the Sinian-Cambrian seawater sulfate (27–32‰; Fig. 10C), but different from those of other geological periods, such as Precambrian (16–18‰), Devonian (~25‰) and modern seawater (~20‰) (Holser, 1977). This indicates that at least part of the sulfur at Zankan was likely sourced from marine sulfates, such as the anhydrite at Zankan (Figs. 2, 4B, E and 5F). From the top to the bottom of the drill core ZK11110, the $\delta^{34}S$ values start at 2.6‰ (257 m deep), increase to 20.4–27.1‰ (293–327 m deep), decrease to 23.9‰ (359 m deep), then increase again to 28.7–32.0‰ (382–437 m deep), and eventually decrease to 18.3–20.3‰ (483–612 m deep) (Fig. 9). This probably reflects the interactions between the hydrothermal fluids and seawater at different mixing ratios.

6.3. Detrital and fluvial input

In the Al_2O_3 vs. SiO_2 discrimination diagram (Fig. 11A), the Zankan ore samples plot across the hydrothermal and hydrogenous fields. This, together with the positive Al_2O_3 vs. SiO_2 correlation, suggests that the precipitation of the Zankan Fe ores was most likely mixed with varying

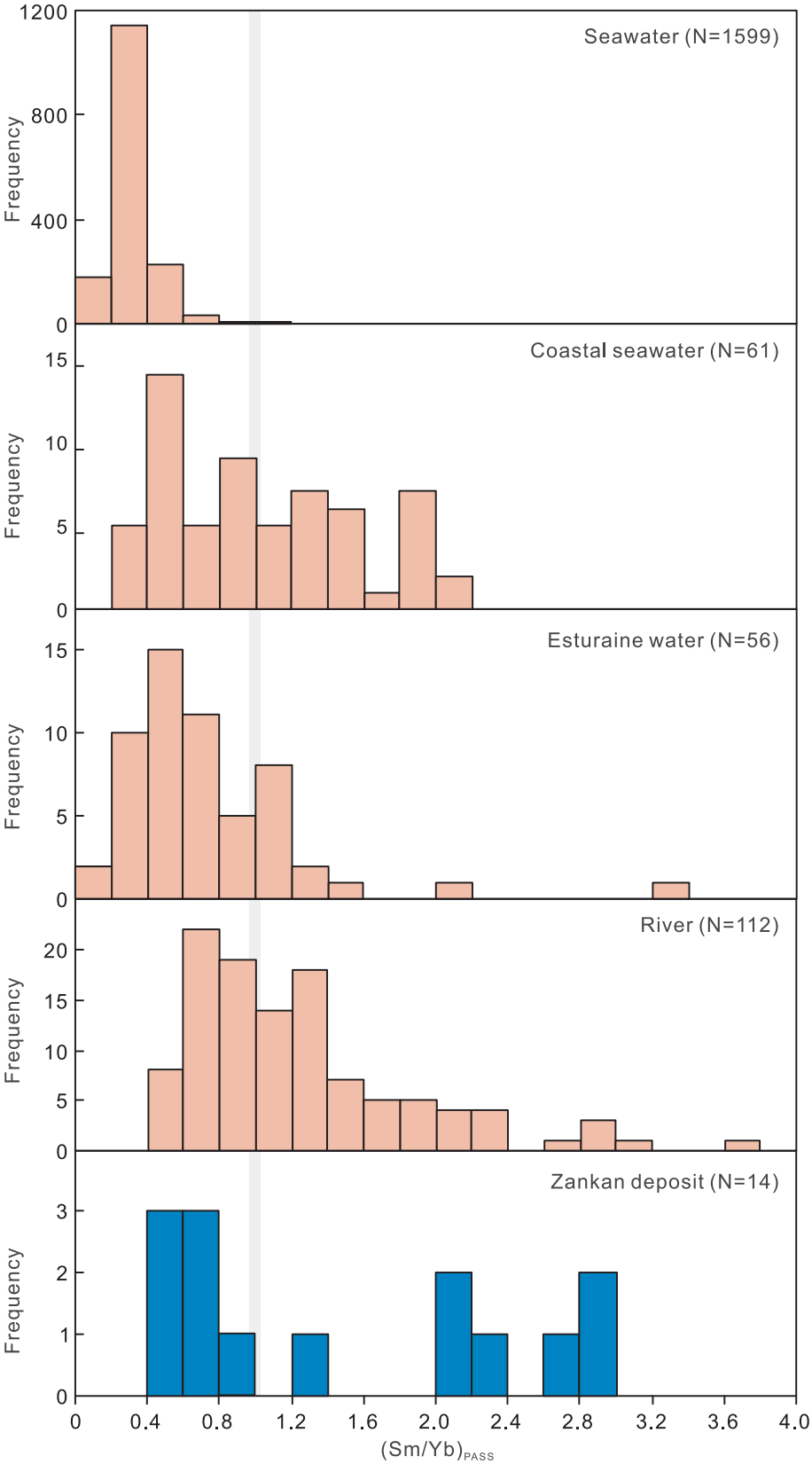

Fig. 12. Histogram of Sm/Yb_{PAAS} values of the Zankan Fe ores. Data sources of seawater: (Elderfield and Greaves, 1982; Klinkhammer et al., 1983; Elderfield and Sholkovitz, 1987; De Baar, 1988; Sholkovitz and Elderfield, 1988; German and Elderfield, 1989, 1990; Tanaka et al., 1990; German et al., 1991; Greaves et al., 1991, 1999; Sholkovitz and Schneider, 1991; Schijf et al., 1991, 1995; Piepgras and Jacobsen, 1992; Westerlund and Oehman, 1992; Sholkovitz, 1993; Mitra et al., 1994; Shimizu et al., 1994; Zhang and Nozaki, 1996, 1998; Bau et al., 1997; Alibo and Nozaki, 1999; Nozaki et al., 1999; Tachikawa et al., 1999, 2004; Alibo and Nozaki, 2000; Amakawa et al., 2000; Hongo and Nozaki, 2001; Haley and Klinkhammer, 2003; Nozaki and Alibo, 2003a,b; Akagi et al., 2004; Censi et al., 2004; Kayasth and Swain, 2004; Lacan and Jeandel, 2004, 2005; Hongo et al., 2006, 2007; Wang and Yamada, 2007; Tazoe et al., 2007; Zhang et al., 2008; Hara et al., 2009; Bayon et al., 2011; Kim and Kim, 2011; Stichel et al., 2012; van de Flierdt et al., 2012; Grenier et al., 2013; Jeande et al., 2013; Garcia-Solsona et al., 2014; Molina-Kescher et al., 2014; Hathorne et al., 2015; Osborne et al., 2015). Data sources of coastal sea, estuarine water and river: (Elderfield and Sholkovitz, 1987; Elderfield et al., 1990; Bertram and Elderfield, 1993; Sholkovitz, 1993; Wang and Liu, 2000; Akagi et al., 2004; Kayasth and Swain, 2004; Wyndham et al., 2004; Han and Liu, 2007; Kim and Kim, 2011).

amount of detritus in a seawater environment (Wonder et al., 1988; González et al., 2009). Aluminum and Ti are considered to be generally immobile during hydrothermal, diagenetic and weathering processes, and the Al_2O_3 and TiO_2 contents can evaluate the terrigenous clastic input, which can increase the Al_2O_3 + TiO_2 values to up to 2% (Kato et al., 1996). The wide range of $Al_2O_3 + TiO_2$ values (0.28–5.48) and HFSE contents (e.g., Zr (3.0–83 ppm), Th (1.49–17.3 ppm) and Hf (< 0.2–2 ppm)) of all the Zankan Fe ore samples indicate various degree of terrigenous clastic input. Ewers and Morris (1981) attributed the TiO_2 vs. Zr correlation to the admixture of a clastic contaminant. At

Zankan, Zr displays a weak correlation against TiO_2 (Fig. 6B), which indicate that crustal clastic input may have been insignificant. Moreover, terrestrial materials (e.g., felsic and basaltic crust), hydrothermal fluids and chondrite have constant Y/Ho ratios of 26–28 (Bau and Dulski, 1999; Webb and Kamber, 2000; Bolhar et al., 2004), and cause co-variation between the Y/Ho ratio and identifying elements of terrestrial crust, (e.g., Al, Zr, Th and Hf). The Zankan ore samples have Y/Ho ratios of 24–30, indicating that the Zankan deposit may have been influenced by detrital contamination and/or hydrothermal fluids. However, the poor correlations between Y/Ho and Zr, Th, Hf and Al_2O_3 contents (Fig. 6C − F) suggest that the Y/Ho ratios are less affected by detrital contamination.

High-temperature (> 250 °C) hydrothermal systems have higher $Eu/Eu*_{PAAS}$ (> 1) and Sm/Yb_{PAAS} ratios than low-temperature (< 250 °C) ones (Pichler et al., 1999; Wheat et al., 2002). The Sm/Yb_{PAAS} values for the seven Zankan ore samples range from 1.25 to 2.87. Three of the seven samples (10–526, A1-02 and PM10-1) exhibit no positive Eu anomalies ($Eu/Eu*_{PAAS}$ = 0.36–0.69; Table 1), implying that the high-temperature hydrothermal fluids had no notable contribution to the Sm/Yb ratios of these three samples. River water generally shows a relatively high REE concentrations and MREE enrichment (e.g., Osborne et al., 2015). The Sm/Yb_{PAAS} values for these three Zankan samples range from 1.25–2.81, which are higher than those of modern seawater (0.03–1.21) (Fig. 12), but overlap with the water in coastal sea (0.32–2.13), estuarine (0.16–3.24), and river (0.44–3.72) (Fig. 12). These three samples show high ΣREY (604–1254 ppm) and MREE enrichment, implying that fluvial input may have also contributed to the formation of Zankan deposit in the shallow sea.

7. Concluding remarks

(1) The Zankan iron deposit is hosted in the pre-Devonian Bulunkuole volcanic-sedimentary succession. The orebodies are stratiform or stratabound. The ores are laminated or banded, and show a unique mineral assemblage of magnetite, pyrite and anhydrite.
(2) The major, trace and rare earth element geochemistry suggest that both high-temperature hydrothermal fluid and seawater contributed to the Zankan Fe mineralization, probably also with terrigenous clastics and fluvial input.
(3) The Zankan Fe ores show a strikingly wide range of $\delta^{34}S$ values (3.2 to 32.8‰), which suggest that the sulfur was derived from different sources. The seawater sulfate was likely to be an important source, and volcanogenic source may have also been present.
(4) The ore geology, geochemistry and sulfur isotopes indicate that the Zankan deposit was probably formed in an Early Cambrian seafloor hydrothermal system.

Acknowledgments

This work was jointly granted by the National Natural Science Foundation of China (Nos. 41402061, 41672086, U1403292), the China Geological Survey Bureau (1212011140056), Scientific Research Fund of the Institute of Geomechanics, CAGS (DZLXJK201606), and National Key Technology Research and Development Program of the Ministry of Science and Technology of China (2015BAB05B04). Drs. Xiaohui Sun, Kunyue Lin, Shidong Mao and Ying Zhang are thanked for their help in the laboratory work. Corrections, comments and suggestions from reviewers and Professors Huayong Chen and F Pirajno greatly improved the quality of the paper.

References

Akagi, T., Hashimoto, Y., Fu, F.F., Tsuno, H., Tao, H., Nakano, Y., 2004. Variation of the distribution coefficients of rare earth elements in modern coral-lattices: species and site dependencies. Geochim. Cosmochim. Acta 68, 2265–2273.
Alibo, D.S., Nozaki, Y., 1999. Rare earth elements in seawater: particle association, shale-normalization, and Ce oxidation. Geochim. Cosmochim. Acta 63, 363–372.
Alibo, D.S., Nozaki, Y., 2000. Dissolved rare earth elements in the South China Sea: Geochemical characterization of the water masses. J. Geophys. Res. 105, 28771–28783.
Amakawa, H., Alibo, D.S., Nozaki, Y., 2000. Nd isotopic composition and REE pattern in the surface waters of the eastern Indian Ocean and its adjacent seas. Geochim. Cosmochim. Acta 64, 1715–1727.
Bau, M., Dulski, P., 1996. Distribution of yttrium and rare-earth elements in the Penge and Kuruman iron-formations, Transvaal Supergroup, South Africa. Precambrian Res. 79, 37–55.
Bau, M., Dulski, P., 1999. Comparing yttrium and rare earths in hydrothermal fluids from the Mid-Atlantic Ridge: implications for Y and REE behaviour during near-vent mixing and for the Y/Ho ratio of Proterozoic seawater. Chem. Geol. 155, 77–90.
Bau, M., Koschinsky, A., Dulski, P., Heinz, J.R., 1996. Comparison of the partitioning behaviors of yttrium, rare earth elements, and titanium between hydrogenetic marine ferromanganese crusts and seawater. Geochim. Cosmochim. Acta 60, 1709–1725.
Bau, M., Moeller, P., Dulski, P., 1997. Yttrium and lanthanides in eastern Mediterranean seawater and their fractionation during redox-cycling. Mar. Chem. 56, 123–131.
Bayon, G., Birot, D., Ruffine, L., Caprais, J.C., Ponzevera, E., Bollinger, C., Donval, J.P., Charlou, J.L., Voisset, M., Grimaud, S., 2011. Evidence for intense REE scavenging at cold seeps from the Niger Delta margin. Earth Planet. Sci. Lett. 312, 443–452.
Bertram, C.J., Elderfield, H., 1993. The geochemical balance of the rare earth elements and neodymium isotopes in the oceans. Geochim. Cosmochim. Acta 57, 1957–1986.
Bolhar, R., Kamber, B.S., Moorbath, S., Fedo, C.M., Whitehouse, M.J., 2004. Characterisation of Early Archean chemical sediments by trace element signatures. Earth Planet. Sci. Lett. 222, 43–60.
Cao, Y., Wang, J., Liu, J.G., Bao, Z.Y., Song, Y., Li, A., 2016. Formation and significance of adakitic rocks in datong pluton of early paleozoic magmatic arc of Western Kunlun Orogen. J. Jilin Univ. (Earth Sci. Ed.) 46, 425–442.
Carew, M.J., 2004. Controls on Cu-Au Mineralisation and Fe Oxide Metasomatism in the Eastern Fold Belt, NW Queensland, Australia (Unpublished thesis). James Cook University, Queensland.
Censi, P., Mazzola, S., Sprovieri, M., Bonanno, A., Patti, B., Punturo, R., Spoto, S.E., Saiano, F., Alonzo, G., 2004. Rare earth elements distribution in seawater and suspended particulate of the Central Mediterranean Sea. Chem. Ecol. 20, 323–343.
Chen, C.J., 2012. Study of Metallogenic Regularity and Prospecting Direction of iron deposit in Taxkorgan area, Xinjiang Province. Master Thesis, China University of Geosciences, Wuhan, 90pp. (in Chinese with English abstract).
Chen, S.Y., 2013. Geological characteristics of the magnetite deposit in Taxkorgan mining area, Xinjiang. Master Thesis, China University of Geosciences, Beijing, 44pp. (in Chinese with English abstract).
Chen, Y.J., Santosh, M., 2014. Triassic tectonics and mineral systems in the Qinling Orogen, central China. Geol. J. 49, 338–358.
Chen, J.K., Yan, C.H., Zhang, W.S., Gao, T.C., Lu, X.H., Zhang, S.B., Hu, X.C., 2011. Geological characteristics and prospecting direction of the magnetite iron deposits in the Taxkorgan, Xinjiang. Geolog. Survey Res. 34, 179–189 (in Chinese with English abstract).
Chen, Y., Wu, L., Zhang, C.J., Cui, X.M., Li, Z.C., Niu, J., 2013. Primary study on geological characteristics of Zankan iron deposit in Tashkurgan in Western Kunlun in Xinjiang Uygur Autonomous Region. Land Res. Shandong Province 29, 18–22 (in Chinese with English abstract).
Chen, Y.J., Santosh, M., Somreville, I.D., Chen, H.Y., 2014. Indosinian tectonics and mineral systems in China: an introduction. Geol. J. 49, 331–337.
De Baar, H.J.W., 1988. Rare earth element distributions in anoxic waters of the Cariaco Trench. Geochim. Cosmochim. Acta 52, 1203–1219.
Dong, L.H., Feng, J., Zhuang, D.Z., Liu, B., Li, F.M., Qu, X., Jiang, Y.H., Zhou, G., 2011. Xinjiang Geological mineral exploration retrospect and prospect. Xinjiang Geol. 29, 1–6 (in Chinese with English abstract).
Dong, L.H., Li, J.H., Feng, J., Zhuang, D.Z., Liu, B., Li, F.M., Qu, X., Jiang, Y.H., 2012. The main Achievement and progress of Xinjiang Geology and Mineral Exploration in 2011. Xinjiang Geol. 30, 1–4 (in Chinese with English abstract).
Dong, L.H., Chen, Y.J., Li, J.H., Qu, X. (eds.), 2016. Precambrian mineralization and exploration targeting in the circum Tarim area. Geological Survey of Xinjiang Uygur Autonomous Region, Urumqi, Research report No. 1212011140056 (in Chinese).
Elderfield, H., Greaves, M.J., 1982. The rare earth elements in seawater. Nature 296, 214–219.
Elderfield, H., Sholkovitz, E.R., 1987. Rare earth elements in the pore waters or reducing nearshore sediments. Earth Planet. Sci. Lett. 82, 280–288.
Elderfield, H., Upstillgoddard, R., Sholkovitz, E.R., 1990. The rare-earth elements in rivers, estuaries, and coastal seas and their significance to the composition of ocean waters. Geochim. Cosmochim. Acta 54, 971–991.
Ewers, W.E., Morris, R.C., 1981. Studies on the Dales Gorge member of Brockman iron formation. Econ. Geol. 76, 1929–1953.
Feng, C.R., Wu, H.C., Chen, Y., 2011. Geological characteristics and genesis of the Zankan iron deposit in Taxkorgan, Xinjiang. Geotectonica et Metallogenia 35, 404–409 (in Chinese with English abstract).
Freslon, N., Bayon, G., Birota, D., Bollinger, C., Barrat, J.A., 2011. Determination of rare earth elements and other trace elements (Y, Mn Co, Cr) in seawater using Tm addition and Mg(OH)2 co-precipitation. Talanta 85, 582–587.
Garcia-Solsona, E., Jeandel, C., Labatut, M., Lacan, L., Vance, D., Chavagnac, V., Pradoux, C., 2014. Rare earth elements and Nd isotopes tracing water mass mixing and particle-seawater interactions in the SE Atlantic. Geochim. Cosmochim. Acta 125, 351–372.
German, C.R., Elderfield, H., 1989. Rare earth elements in Saanich Inlet, British Columbia, a seasonally anoxic basin. Geochim. Cosmochim. Acta 53, 2561–2571.
German, C.R., Elderfield, H., 1990. Rare earth elements in the NW Indian Ocean. Geochim. Cosmochim. Acta 54, 1929–1940.
German, C.R., Holliday, B.P., Elderfield, H., 1991. Redox cycling of rare earth elements in the suboxic zone of the Black Sea. Geochim. Cosmochim. Acta 55, 3553–3558.
González, P.D., Sato, A.M., Llambías, E.J., Petronilho, L.A., 2009. Petrology and geochemistry of the banded iron formation in the Eastern Sierras Pampeanas of San Luis (Argentina): implications for the evolution of the Nogolí Metamorphic Complex. J. S.

Am. Earth Sci. 28, 89–112.
Greaves, M.J., Rudnicki, M., Elderfield, H., 1991. Rare earth elements in the Mediterranean Sea and mixing in the Mediterranean outflow. Earth Planet. Sci. Lett. 103, 169–181.
Greaves, M.J., Elderfield, H., Sholkovitz, E.R., 1999. Aeolian sources of rare earth elements to the Western Pacific Ocean. Mar. Chem. 68, 31–38.
Grenier, M., Jeandel, C., Lacan, F., Vance, D., Venchiarutti, C., Cros, A., Cravatte, S., 2013. From the subtropics to the central equatorial Pacific Ocean: Neodymium isotopic composition and rare earth element concentration variations. J. Geophy. Res. Oceans 118, 1–27.
Gross, G.A., Mcleod, C.R., 1980. A preliminary assessment of the chemical composition of iron formations in Canada. Can. Mineral. 18, 223–229.
Han, G.L., Liu, C.Q., 2007. Dissolved rare earth elements in river waters draining karst terrains in Guizhou Province. China. Aquat. Geochem. 13, 95–107.
Haley, B.A., Klinkhammer, G.P., 2003. Complete separation of rare earth elements from small volume seawater samples by automated ion chromatography: method development and application to benthic flux. Mar. Chem. 82, 197–220.
Hara, Y., Obata, H., Doi, T., Hong, Y., Gamo, T., Takeda, S., Tsuda, A., 2009. Rare earth elements in seawater during an iron-induced phytoplankton bloom of the western subarctic Pacific (SEEDS-II). Deep Sea Res. Part II 56, 2839–2851.
Hathorne, E.C., Stichel, T., Brück, B., Frank, M., 2015. Rare earth element distribution in the Atlantic sector of the Southern Ocean: The balance between particle scavenging and vertical supply. Mar. Chem. 177, 157–171.
Hoefs, J., 1997. Stable Isotope Geochemistry, 4th edition. Springer-Verlag, Berlin, pp. 201.
Holser, W.T., 1977. Catastrophic chemical events in the history of the ocean. Nature 267, 403–408.
Hongo, Y., Nozaki, Y., 2001. Rare earth element geochemistry of hydrothermal deposits and Calyptogena shell from the Iheya Ridge vent field, Okinawa Trough. Geochem. J. 35, 347–354.
Hongo, Y., Obata, H., Alibo, D.S., Nozaki, Y., 2006. Spatial variations of rare earth elements in North Pacific surface water. J. Oceanogr. 62, 441–455.
Hongo, Y., Obata, H., Gamo, T., Nakaseama, M., Ishibashi, J., Konno, U., Saegusa, S., Ohkubo, S., Tsunogai, U., 2007. Rare earth elements in the hydrothermal system at Okinawa Trough back-arc basin. Geochem. J. 41, 1–15.
Hu, L., 2014. Geological characteristics and prospecting direction of the magnetite deposit in Laobing mining area, Xinjiang. Master Thesis, China University of Geosciences, Beijing, 66pp. (in Chinese with English abstract).
Jeande, C., Delattre, H., Grenier, M., Pradoux, C., Lacan, F., 2013. Rare earth element concentrations and Nd isotopes in the Southeast Pacific Ocean. Geochem. Geophys. Geosyst. 14, 328–341.
Ji, W.H., Li, R.S., Chen, C.J., He, S.P., Zhao, Z.M., Bian, X.W., Zhu, H.P., Cui, J.G., Ren, J.G., 2011. The discovery of Palaeoproterozoic volcanic rocks in the Bulunkuoler Group from the Tianshuihai Massif in Xinjiang of Northwest China and its geological significance. Sci. China Earth Sci. 54, 61–72.
Jia, R.Y., Jiang, Y.H., Liu, Z., Zhao, P., Zhou, Q., 2013. Petrogenesis and tectonic implications of early Silurian high-K calc-alkaline granites and their potassic microgranular enclaves, western Kunlun orogen, NW Tibetan Plateau. Int. Geol. Rev. 55, 958–975.
Jiang, Y.H., Jia, R.Y., Liu, Z., Liao, S.Y., Zhao, P., Zhou, Q., 2013. Origin of Middle Triassic high-K calc-alkaline granitoids and their potassic microgranular enclaves from the western Kunlun orogen, northwest China: a record of the closure of Paleo-Tethys. Lithos 156–159, 13–30.
Kato, Y., Kawakami, T., Kano, T., Kunugiza, K., Swamy, N.S., 1996. Rare-earth element geochemistry of banded iron formations and associated amphibolite from the Sargur belts, south India. J. Southeast Asian Earth Sci. 14, 161–164.
Kayasth, K., Swain, K., 2004. Determination of rare-earth elements in Periyar River water (Kerala, India) and seawater (Mumbai, India) using neutron activation analysis. J. Radioanal. Nucl. Chem. 262, 191–194.
Kim, I., Kim, G., 2011. Large fluxes of rare earth elements through submarine groundwater discharge (SGD) from a volcanic island, Jeju. Korea. Mar. Chem. 127, 12–19.
Klinkhammer, G., Elderfield, H., Hudson, A., 1983. Rare earth elements in seawater near hydrothermal vents. Nature 305, 185–188.
Lacan, F., Jeandel, C., 2004. Neodymium isotopic composition and rare earth element concentrations in the deep and intermediate Nordic Seas: constraints on the Iceland Scotland Overflow water signature. Geochem. Geophys. Geosyst. 5, Q11006.
Lacan, F., Jeandel, C., 2005. Acquisition of the neodymium isotopic composition of North Atlantic Deep Water. Geochem. Geophys. Geosyst. 6, Q12008.
Li, W.H., Yang, C.M., 1983. Palaeotectonic and geochemical environment of Precambrian submarine volcanic sedimentary metamorphic iron ore in Luan Xian of the Eastern Hebei Province. Earth Sci. 3, 117–126 (in Chinese with English abstract).
Li, N., Pirajno, F., 2017. Early Mesozoic Mo mineralization in the Qinling Orogen: an overview. Ore Geol. Rev. 81, 431–450.
Li, N., Chen, Y.J., Santosh, M., Pirajno, F., 2015a. Compositional polarity of Triassic granitoids in the Qinling Orogen, China: Implication for termination of the northernmost paleo-Tethys. Gondwana Res. 27, 244–257.
Li, H.Z., Zhai, M.G., Zhang, L.C., Li, Z.Q., Zheng, M.T., Niu, J., Yu, P.P., 2015b. Study on geochemistry and micro-area characteristics of Paleoproterozoic chemical sedimentary rocks from Zankan area, West Kunlun, China. Acta Petrologica Sinica 32, 233–250 (in Chinese with English abstract).
Li, Z.Q., Zhang, L., Xue, C.J., Zheng, M.T., Hao, Y.H., Shi, Y.J., 2015c. Geological and geochemical characteristics of Zankan iron deposit in the West Kunlun Mountains. Chinese J. Geol. 50, 100–117 (in Chinese with English abstract).
Liao, S.Y., Jiang, Y.H., Jiang, S.Y., Yang, W.Z., Zhou, Q., Jin, G.D., Zhao, P., 2010. Subducting sediment-derived arc granitoids: evidence from the Datong pluton and its quenched enclaves in the western Kunlun orogen, northwest China. Mineral. Petrol. 100, 55–74.
Lin, S.K., 2015. Study on geochemistry and zirocn U-Pb ages of dacite porphyry from the Zankan iron deposit, West Kunlun area. Master Thesis, Kunming University of Science and Technology, Kunming, 64pp. (in Chinese with English abstract).
Liu, Z., Jiang, Y.H., Jia, R.Y., Zhao, P., Zhou, Q., Wang, G.C., Ni, C.Y., 2014. Origin of Middle Cambrian and Late Silurian potassic granitoids from the western Kunlun orogen, northwest China: a magmatic response to the Proto-Tethys evolution. Miner. Petrol. 108, 91–110.
Mao, S.D., Chen, Y.J., Zhou, Z.J., Lu, Y.H., Guo, J.H., Qin, Y., Yu, J.Y., 2014. Zircon geochronology and Hf isotope geochemistry of the granitoids in the Yangshan gold field, western Qinling, China: implications for petrogenesis, ore genesis and tectonic setting. Geol. J. 49, 359–382.
Mattern, F., Schneider, W., 2000. Suturing of the Proto- and Paleo-Tethyan oceans in the western Kunlun (Xinjiang, China). J. Asian Earth Sci. 18, 637–650.
McLennan, S., 1989. Rare earth elements in sedimentary rocks; influence of provenance and sedimentary processes. Rev. Mineral. Geochem. 21, 169–200.
Mi, M., Chen, Y.J., Yang, Y.F., Wang, P., Xu, Y.L., Li, F.L., Wan, S.Q., 2015. Geochronology and geochemistry of the giant Qian'echong Mo deposit, Dabie Shan, eastern China: implications for ore genesis and tectonic setting. Gondwana Res. 27, 1217–1235.
Mitra, A., Elderfield, H., Greaves, M.J., 1994. Rare earth elements in submarine hydrothermal fluids and plumes from the Mid-Atlantic Ridge. Mar. Chem. 46, 217–235.
Molina-Kescher, M., Frank, M., Hathorne, E., 2014. South Pacific dissolved Nd isotope compositions and rare earth element distributions: water mass mixing versus biogeochemical cycling. Geochim. Cosmochim. Acta 127, 171–189.
Nath, B.B., Pluger, W.L., Roelandts, I., 1997. Geochemical constraints on the hydrothermal origin of ferromanganese incrustations from the Rodriguez triple junction, Indian Ocean. In: In: Nicholson, K., Hein, J.R., Buhn, B., Dasgupta, S. (Eds.), Manganese Mineralization: Geochemistry and Mineralogy of Terrestrial and Marine Deposits Geological Society, London, pp. 199–211 (Special Publication 119).
Nicholson, K., 1992. Contrasting mineralogical-geochemical signatures of manganese oxides: guides to metallogenesis. Econ. Geol. 87, 1253–1264.
Nijman, W., de Bruijne, K., Valkering, M.E., 1998. Growth fault control of Early Archaean cherts, barite mounds and chert–barite veins, North Pole Dome, Eastern Pilbara, Western Australia. Precambrian Res. 88, 25–52.
Nozaki, Y., Alibo, D.S., 2003a. Importance of vertical geochemical processes in controlling the oceanic profiles of dissolved rare earth elements in the northeastern Indian Ocean. Earth Planet. Sci. Lett. 205, 155–172.
Nozaki, Y., Alibo, D.S., 2003b. Dissolved rare earth elements in the Southern Ocean, southwest of Australia: unique patterns compared to the South Atlantic data. Geochem. J. 37, 47–62.
Nozaki, Y., Alibo, D.S., Amakawa, H., Gamo, T., Hasumoto, H., 1999. Dissolved rare earth elements and hydrography in the Sulu Sea. Geochim. Cosmochim. Acta 63, 2171–2181.
Oksuz, N., 2011. Geochemical characteristics of the Eymir (Sorgun-Yozgat) manganese deposit. J. Rare Earth 29, 287.
Osborne, A.H., Haley, B.A., Hathorne, E.C., Plancherel, Y.P., Frank, M., 2015. Rare earth element distribution in Caribbean seawater: Continental inputs versus lateral transport of distinct REE compositions in subsurface water masses. Mar. Chem. 177, 172–183.
Pan, Y.S., Wang, Y., 1994. Tectonic evolution along the geotraverse from Yecheng to Shiquanhe. Acta Geol. Sinica 68, 295–307 (in Chinese).
Pan, Y.S., Bian, Q.T., 1996. Tectonics. In: Pan, Y.S. (Ed.), Geologic Evolution of the Karakorum and Kunlun Mountains. Seismological Press, Beijing, pp. 187–229.
Pichler, T., Veizer, J., Hall, G.E.M., 1999. The chemical composition of shallow-water hydrothermal fluids in Tutum Bay, Ambitle Island, Papua New Guinea and their effect on ambient seawater. Mar. Chem. 64, 229–252.
Piepgras, D.J., Jacobsen, S.B., 1992. The behavior of rare earth elements in seawater: precise determination of variations in the North Pacific water column. Geochim. Cosmochim. Acta 56, 1851–1862.
Qi, L., Gregoire, D.C., 2000. Determination of trace elements in twenty six Chinese geochemistry reference materials by inductively coupled plasma-mass spectrometry. Geostand. Newslett. 24, 51–63.
Qian, B., Gao, Y.B., Li, K., Zhang, Z.W., Hao, Y.H., 2014. Mineralogy and genesis of the Zankan iron deposit in Taxkorgan area' Xinjiang. Geol. Exploration 50, 630–640 (in Chinese with English abstract).
Qiao, G.B., Wang, P., Wu, Y.Z., Wu, Y.A., Hao, Y.H., Zhao, X.J., Chen, D.H., Lv, P.R., Du, W., 2015. Formation age of ore-bearing strata of the Zankan iron deposit in Taxkorgan landmass of Western Kunlun Mountains and its geological significance. Geol. China 42, 616–630 (in Chinese with English abstract).
Ren, G.L., Li, J.Q., Wang, H., Liu, J.P., Gao, T., Yang, M., Yi, H., Han, H.H., Yang, J.L., 2013. The Metallogenic series of iron deposits in Bulunkou-Zankan, west Kunlun. Xinjiang Geol. 31, 318–323 (in Chinese with English abstract).
Schijf, J., de Baar, H.J.W., Wijbrans, J.R., Landing, W.M., 1991. Dissolved rare earth elements in the Black Sea. Deep Sea Res. 38 (Suppl. 2), S805–S823.
Schijf, J., de Baar, H.J.W., Millero, F.J., 1995. Vertical distribution and speciation of dissolved rare earth elements in the anoxic brines of Bannock Basin, eastern Mediterranean Sea. Geochim. Cosmochim. Acta 59, 3285–3299.
Shimizu, H., Tachikawa, K., Masuda, A., Nozaki, Y., 1994. Cerium and neodymium isotope ratios and REE patterns in seawater from the North Pacific Ocean. Geochim. Cosmochim. Acta 58, 323–333.
Sholkovitz, E.R., 1993. The geochemistry of rare earth elements in the Amazon River estuary. Geochim. Cosmochim. Acta 57, 2181–2190.
Sholkovitz, E.R., Elderfield, H., 1988. Cycling of dissolved rare earth elements in Chesapeake Bay. Global Biogeochem. Cycles 2, 157–176.
Sholkovitz, E.R., Schneider, D.L., 1991. Cerium redox cycles and rare earth elements in the Sargasso Sea. Geochim. Cosmochim. Acta 55, 2737–2743.
Stichel, T., Frank, M., Rickli, J., Hathorne, E.C., Haley, B.A., Jeandel, C., Pradoux, C., 2012. Sources and input mechanisms of hafnium and neodymium in surface waters of the Atlantic sector of the Southern Ocean. Geochim. Cosmochim. Acta 94, 22–37.
Sun, H.T., Li, C.J., Wu, H., Wang, H.J., Qi, S.J., Chen, G.M., Liu, Z.T., Gao, P., 2003. Overview of Metallogenesis on Western Kunlun. Geological Publishing House, Beijing, 251pp. (in Chinese).
Surya Prakash, L., Ray, D., Paropkari, A.L., Mudholkar, A.V., Satyanarayanan, M., Sreenivas, B., Chandrasekharam, D., Kota, D., Raju, K.A.K., Kaisary, S., Balaram, V., Gurav, T., 2012. Distribution of REEs and yttrium among major geochemical phases

of marine Fe-Mn-oxides: comparative study between hydrogenous and hydrothermal deposits. Chem. Geol. 312–313, 127–137.
Tachikawa, K., Jeandel, C., Roy-Barman, M., 1999. A new approach to the Nd residence time in the ocean: the role of atmospheric inputs. Earth Planet. Sci. Lett. 170, 433–446.
Tachikawa, K., Roy-Barman, M., Michard, A., Thouron, D., Yeghicheyan, D., Jeandel, C., 2004. Neodymium isotopes in the Mediterranean Sea: Comparison between seawater and sediment signals. Geochim. Cosmochim. Acta 68, 3095–3106.
Tanaka, M., Shimizu, H., Masuda, A., 1990. Features of the heavy rare-earth elements in seawater. Geochem. J. 24, 39–46.
Tazoe, H., Obata, H., Amakawa, H., Nozaki, Y., Gamo, T., 2007. Precise determination of the cerium isotopic compositions of surface seawater in the Northwest Pacific Ocean and Tokyo Bay. Mar. Chem. 103, 1–14.
van de Flierdt, T., Pahnke, K., Amakawa, H., Andersson, P., Basak, C., Coles, B., Colin, C., Crocket, K., Frank, M., Frank, N., Goldstein, S.L., Goswami, V., Haley, B.A., Hathorne, E.C., Hemming, S.R., Henderson, G.M., Jeandel, C., Jones, K., Kreissig, K., Lacan, F., Lambelet, M., Martin, E.E., Newkirk, D.R., Obata, H., Pena, L., Piotrowski, A.M., Pradoux, C., Scher, H.D., Schöberg, H., Singh, S.K., Stichel, T., Tazoe, H., Vance, D., Yang, J., 2012. GEOTRACES intercalibration of neodymium isotopes and rare earth element concentrations in seawater and suspended particles. Part 1: reproducibility of results for the international intercomparison. Limnol. Oceanogr.: Methods 10, 234–251.
Wang, Z.L., Liu, C.Q., 2000. Distributions of dissolved rare earth elements during estuarine mixing at the Changjiang River mouth. Chin. Sci. Bull. 45, 1795–1799.
Wang, Z.L., Yamada, M., 2007. Geochemistry of dissolved rare earth elements in the Equatorial Pacific Ocean. Environ. Geol. 52, 779–787.
Wang, P., Chen, Y.J., Fu, B., Yang, Y.F., Mi, M., Li, Z.L., 2014. Fluid inclusion and H-O-C isotope geochemistry of the Yaochong porphyry Mo deposit in Dabie Shan, China: A case study of porphyry systems in continental collision orogens. Int. J. Earth Sci. 103, 777–797.
Wang, C.M., Zhang, L., Tang, H.S., Chen, H.Y., Li, X.L., Zheng, Y., Li, D.F., Fang, J., Dong, L.H., Qu, X., 2017a. Genesis of the Kaladawan Fe–Mo ore field in Altyn, Xinjiang, China: Constraints from mineralogy and geochemistry. Ore Geol. Rev. 81, 587–601.
Wang, P., Wang, Y., Yang, Y.F., 2017b. Zircon U-Pb geochronology and isotopic geochemistry of the Tangjiaping Mo deposit, Dabie Shan, China: Implications for ore genesis and tectonic setting. Ore Geol. Rev. 81, 466–483.
Webb, G.E., Kamber, B.S., 2000. Rare earth elements in Holocene reefal microbialites: a new shallow seawater proxy. Geochim. Cosmochim. Acta 64, 1557–1565.
Westerlund, S., Oehman, P., 1992. Rare earth elements in the Arctic Ocean. Deep Sea Res. 39, 1613–1626.
Wheat, C.G., Mottl, M.J., Rudnicki, M., 2002. Trace element and REE composition of a low-temperature ridge-flank hydrothermal spring. Geochim. Cosmochim. Acta 66, 3693–3705.
Wonder, J., Spry, P., Windom, K., 1988. Geochemistry and origin of manganese-rich rocks related to iron-formation and sulfide deposits, western Georgia. Econ. Geol. 83, 1070–1081.
Wyndham, T., McCulloch, M., Fallon, S., Alibert, C., 2004. High-resolution coral records of rare earth elements in coastal seawater: biogeochemical cycling and a new environmental proxy. Geochim. Cosmochim. Acta 68, 2067–2080.
Xiao, W.J., Hou, Q.L., Li, J.L., 2000. Tectonic facies and the archipelago-accretion process of the West Kunlun. China. Sci. China Ser. D (supp.) 43, 134–143.
Xiao, W.J., Windley, B.F., Liu, D.Y., Jian, P., Liu, C.Z., Yuan, C., Sun, M., 2005. Accretionary tectonics of the Western Kunlun Orogen, China: a Paleozoic-early Mesozoic, long-lived active continental margin with implications for the growth of Southern Eurasia. J. Geol. 113, 687–705.
Xu, R.H., Zhang, Y.Q., Xie, Y.W., Chen, F.K., Vadal, P., Nicolas, A., Zhang, Q.D., Zhao, D.M., 1994. A discovery of an early Palaeozoic tectonomagmatic belt in the northern part of west Kunlun mountains. Scientia Geologica Sinica 4, 313–328 (in Chinese with English abstract).
Yan, C.H., Cao, X.Z., Zhang, W.S., Chen, J.K., Liu, B.D., Wang, S.Y., Zhang, S.B., Li, S.P., Liu, S.J., 2012a. The "Pamir-type" iron deposits. Geological Publishing House, Beijing, 256pp. (in Chinese).
Yan, C.H., Chen, C.J., Cao, X.Z., Zhang, W.S., Chen, J.K., Li, S.P., Liu, P.D., 2012b. The discovery of the "Pamir-type" iron deposits in Taxkorgan area of Xinjiang and its geological significance. Geological Bulletin of China 31, 549–557 (in Chinese with English abstract).
Yang, W.Q., 2013. The Indosinian metamorphism, magmatism and formation age of Bunlunkuole rock group in Taxkorgan-Kangxiwa tectonic belt, Western Kunlun (Ph.D. Thesis). Northwest University, Xian 128pp (in Chinese with English abstract).
Yang, Y.F., Wang, P., 2017. Geology, geochemistry and tectonic settings of molybdenum deposits in southwestern China: a review. Ore Geol. Rev. 81, 965–995.
Yang, W.Q., Liu, L., Cao, Y.T., Wang, C., He, S.P., Li, R.S., Zhu, X.H., 2010. Geochronological evidence of Indosinian (high-pressure) metamorphic event and its tectonic significance in Taxkorgan area of the Western Kunlun Mountains. NW China. Sci. China Earth Sci. 53, 1445–1459.
Zarasvandi, A., Lentz, D., Rezaei, M., Pourkaseb, H., 2013. Genesis of the Nasirabad manganese occurrence, Fars province, Iran: Geochemical evidences. Chem. Erde 73, 495–508.
Zhang, J., Nozaki, Y., 1996. Rare earth elements and yttrium in seawater: ICP-MS determinations in the East Caroline, Coral Sea, and South Fiji basins of the western South Pacific Ocean. Geochim. Cosmochim. Acta 60, 4631–4644.
Zhang, J., Nozaki, Y., 1998. Behavior of rare earth elements in seawater at the ocean margin: a study along the slopes of the Sagami and Nankai troughs near Japan. Geochim. Cosmochim. Acta 62, 1307–1317.
Zhang, C.L., Lu, S.N., Yu, H.F., Ye, H.M., 2007. Tectonic evolution of Western Orogenic belt: evidences from zircon SHRIMP and LA–ICP–MS U-Pb ages. Sci. China Ser. D Earth Sci. 37, 145–154.
Zhang, Y., Lacan, F., Jeandel, C., 2008. Dissolved rare earth elements tracing lithogenic inputs over the Kerguelen Plateau (Southern Ocean). Deep Sea Res. Part II 55, 638–652.
Zheng, Z., Deng, X.H., Chen, H.J., Yue, S.W., Dong, L.H., Qu, X., Chen, Y.J., 2016. Fluid sources and metallogenesis in the Baiganhu W-Sn deposit, East Kunlun, NW China: Insights from chemical and boron isotopic compositions of tourmaline. Ore Geol. Rev. 72, 1129–1142.
Zhou, Z.J., Chen, Y.J., Jiang, S.Y., Zhao, H.X., Qin, Y., Hu, C.J., 2014a. Geology, geochemistry and ore genesis of the Wenyu gold deposit, Xiaoqinling gold field, southern margin of North China Craton. Ore Geol. Rev. 59, 1–20.
Zhou, Z.J., Liu, Z.W., Qin, Y., 2014b. Geology, geochemistry and genesis of the Huachanggou gold deposit, western Qinling Orogen, central China. Geol. J. 49, 424–441.
Zhou, Z.J., Chen, Y.J., Jiang, S.Y., Hu, C.J., Qin, Y., Zhao, H.X., 2015. Isotope and fluid inclusion geochemistry and ore genesis of the Qiangma gold deposit, Xiaoqinling gold field, Qinling Orogen, southern margin of North China Craton. Ore Geol. Rev. 66, 47–64.
Zhou, Z.J., Mao, S.D., Chen, Y.J., Santosh, M., 2016. U-Pb ages and Lu-Hf isotopes of detrital zircons from the southern Qinling Orogen: implications for Precambrian to Phanerozoic tectonics in central China. Gondwana Res. 35, 323–337.
Zhou, Z.J., Tang, H.S., Chen, Y.J., Chen, Z.L., 2017. Trace elements of magnetite and iron isotopes of the Zankan iron deposit, westernmost Kunlun, China: A case study of seafloor hydrothermal iron deposits. Ore Geol. Rev. 80, 1191–1205.